Atmospheric Research 248 (2021) 105200

Contents lists available at ScienceDirect

Atmospheric Research

journal homepage: www.elsevier.com/locate/atmosres

Analysis of long-term potential gradient variations measured in the Argentinian Andes

J. Tacza[a,*], J.-P. Raulin[a], C.A. Morales[b], E. Macotela[c], A. Marun[d], G. Fernandez[e]

[a] Center of Radio Astronomy and Astrophysics Mackenzie, Engineering School, Mackenzie Presbyterian University, São Paulo, SP, Brazil
[b] Institute of Astronomy, Geophysics and Atmospheric Science, Department of Atmospheric Science, University of São Paulo, São Paulo, SP, Brazil
[c] Sodankyla Geophysical Observatory, University of Oulu, Sodankyla, Finland
[d] Instituto de Ciencias Astronómicas de la Tierra y el Espacio, ICATE-CONICET-UNSJ, San Juan, Argentina
[e] Complejo Astronómico El Leoncito, CASLEO, San Juan, Argentina

ARTICLE INFO

Keywords:
Aerosols
Atmospheric electric field
Global electric circuit
Austausch process
Convective process

ABSTRACT

Continuous measurements of the potential gradient are being recorded at the CASLEO astronomical observatory near to the Andes Mountain of Argentina, since 2010 (Latitude: 31°47.88′S, Longitude: 69°17.7′W, Altitude: 2552 masl). This study aims to use the potential gradient diurnal variation in fair weather conditions, which we named 'standard curve', to examine its correlation with the 'universal' Carnegie curve and to investigate its dependence with aerosol amount and lightning occurrences. In addition, a spectral analysis was performed to our data. The aerosol optical depth is recorded by an AERONET station at CASLEO, while the lightning occurrences was obtained from the STARNET network. For the analysis, the average of monthly, seasonal and annual electric field curves was determined. We found that the shape of these curves is preserved from year to year indicating their high reliability. The correlation between the standard curve for CASLEO and the Carnegie curve was found to be high ($r = 0.94$). However, some significant local effects were also found. We determined that these local effects in the standard curve may be associated to the convective process, which is more predominant during summertime than wintertime. The inspection of the seasonal variation of the potential gradient and the lightning occurrences showed a high similarity only after removing the effects of aerosols. Apart from this, the spectral analysis exposed a daily, annual and 165-day oscillation in the potential gradient.

1. Introduction

Early studies confirmed the presence of an atmospheric electric field (usually represented in measurements in terms of the Potential Gradient (PG), where $PG = -E_z$) in fair weather regions[1] (Parsons and Mazeas, 1753; Canton, 1753) and further investigation was performed using data measured over the oceans worldwide between 1909 and 1929 (Torreson et al., 1946). On board a ship, the PG was measured every hour over the world's oceans in fair weather conditions. After the daily average of the PG measurements, it was found a daily variation in Universal Time, independent of the ship's position. This daily variation is known as the Carnegie curve, and shows a minimum time and maximum time around 3 UT and 19 UT, respectively. In fair weather, the PG mean value is about −130 V/m (Harrison, 2013).

According to the global electric circuit (GEC) model, the PG in fair weather regions is sustained by electrical "batteries" occurring in disturbed weather regions. The GEC model was first proposed by CTR Wilson (1903, 1921) and is well explained in several reviews (Rycroft et al., 2000; Rycroft et al., 2008; Haldoupis et al., 2017 and reference therein). In essence, this model is the link between disturbed and fair weather regions. The model considers the Earth as a spherical capacitor where the plates are the surface of the Earth and the lower atmosphere. In this circuit there are currents flowing from the cloud's top to the ionosphere, in disturbed weather regions, which flow free through the ionosphere to fair weather regions where these currents flow downward to the ground. These currents flow through the Earth's surface closing the circuit. The global circuit model was first supported by the work of Whipple (1929) which showed a high similarity in the hourly diurnal

* Corresponding author.
E-mail address: josect1986@gmail.com (J. Tacza).

[1] In a recent work, Harrison and Nicoll (2018) proposed as fair weather conditions days without hydrometeors, visual range greater than 2 km, cumuliform cloud less than 3/8, low stratus cloud with its cloud base below 1.5 km and wind speed between 1 m/s and 8 m/s.

https://doi.org/10.1016/j.atmosres.2020.105200
Received 7 April 2020; Received in revised form 11 July 2020; Accepted 12 August 2020
Available online 14 August 2020

variation between the thunderstorm's activity worldwide and the Carnegie curve. This similarity is higher if we add the contribution of the electrical shower clouds to the circuit (Peterson et al., 2017 and references therein). A similar seasonal variation has also been found between the electrical activity and the Carnegie curve, i.e., higher values between June and August and lower values between December and February (Adlerman and Williams, 1996; Markson, 2007; Burns et al., 2012). This seasonal variation is related to the amount of lightning occurring in the summer in the Northern Hemisphere that is larger to that of the Southern Hemisphere due to greater warming experienced over land (Christian et al., 2003).

The study of the GEC behavior is important due to its relationship with several phenomena, such as the role of lightning as generator for the circuit, the evidence of nuclear weapon test and the impact of the tropical 'El Nino Southern Oscillation' on the circuit (Williams, 2009; Williams and Mareev, 2014). The GEC was also proposed to act as a link in the solar influences on the troposphere (Rycroft et al., 2012). Furthermore, the study of the GEC has been suggested as indicator of global warming (Markson, 1986; Williams, 1992; Price, 1993). Therefore, it is important to monitor the global electric circuit continuously. This can be performed through measurements of the PG at the Earth's surface under fair weather conditions. In order to verify whether the global electric circuit is being measured at a specific location, the 'universal' Carnegie curve is generally adopted as the reference curve for comparison. For the validation, one focuses in three parameters: the amplitude variation, the minimum and maximum times and the linear correlation coefficient between the electrical measurement (e.g., PG or thunderstorm daily variation) and the Carnegie curve (Mezuman et al., 2014).

Several sensors to monitor the atmospheric electric field have been installed worldwide in an attempt to reproduce the 'classic Carnegie curve' (Harrison, 2003; Tammet, 2009; Tacza et al., 2014; Jeeva et al., 2016; Yaniv et al., 2016; Burns et al., 2017; Lucas et al., 2017; Yaniv et al., 2017; Nicoll et al., 2019; Gurmani et al., 2020). However, PG measurements on the ground are influenced by several local natural and anthropogenic phenomena, such as (i) aerosols, which change electrical conductivity; (ii) the electrode effect at sites with low ionization sources, which creates a positive electric charge concentrated in the first meters on the ground, and that through turbulence produces between 10 and 50% of variations in the intensity of the PG (Markson, 1975); (iii) electric charges emitted by motors, fires and industry; (iv) PG changes due to the low conductivity of clouds; (v) cloud electrification; (vi) modulation of the electric field by tall objects in the vicinity of the sensor; (vii) variations in the electrical conductivity due to fluctuations in the ion mobility affected by changes in relative humidity (Markson et al., 1999), among others (Markson, 2007 and references therein). These local effects generate deviation in the PG under fair weather conditions when compared with the 'universal' Carnegie curve (Harrison and Aplin, 2002; Harrison, 2006; Silva et al., 2014; Kamogawa et al., 2015; Yaniv et al., 2017; Nicoll et al., 2019).

Deviations due to local effects can be reduced with PG measurements performed at isolated and remote sites, for example in polar regions (Reddell et al., 2004; Kubicki et al., 2016; Burns et al., 2017), mountains (Cobb, 1968; Reiter, 1971; Kamogawa et al., 2015; Yaniv et al., 2017) and islands (Lopes et al., 2017). However, PG measurements on land can still be affected by ground surface ionization sources produced by the emanation of radioactive gases and the natural radioactivity of the soil (the ionization rate being dependent on soil type). These changes in ionization rate produce changes in the electrical conductivity. At nighttime, the electrode effect can produce a buildup of electric charge on the ground when turbulence and wind speed are low. At sunrise, the temperature begins to increase at the Earth's surface, increasing convection and turbulence. These processes increase the concentration of aerosol particles producing a decrease of the electrical conductivity and, by Ohm's law, an increase of the electric field. This phenomenon is known as 'electric agitation' (Israël, 1959) or 'Austausch' process (Kasemir, 1972). Yaniv et al. (2017) noted that the 'Austausch' process was the main local effect producing deviation in the PG in fair weather regions on mountains (located in Israel, Armenia and Switzerland) when compared with the Carnegie curve. A related phenomenon is the 'sunrise' effect, which is an enhancement on the PG after the sunrise (Nichols, 1916; Marshall et al., 1999; Smirnov et al., 2012). Marshall et al. (1999) proposed that this enhancement is due to the accumulation of positive electrode layer before sunrise very close to the ground because little radioactivity of the soil. Upward mixing of the charge after sunrise, produces the enhancement on the PG values. Similarly, Smirnov et al. (2012) proposed that the sunrise effect is related to the turbulence and convection processes in the planetary boundary

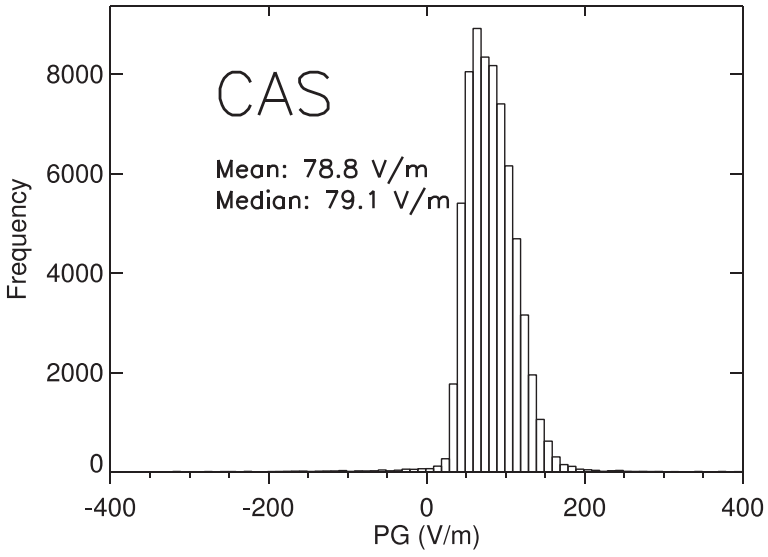

Fig. 1. Histogram of the PG hourly values for CAS station (plotted within a range of ± 400 V/m).

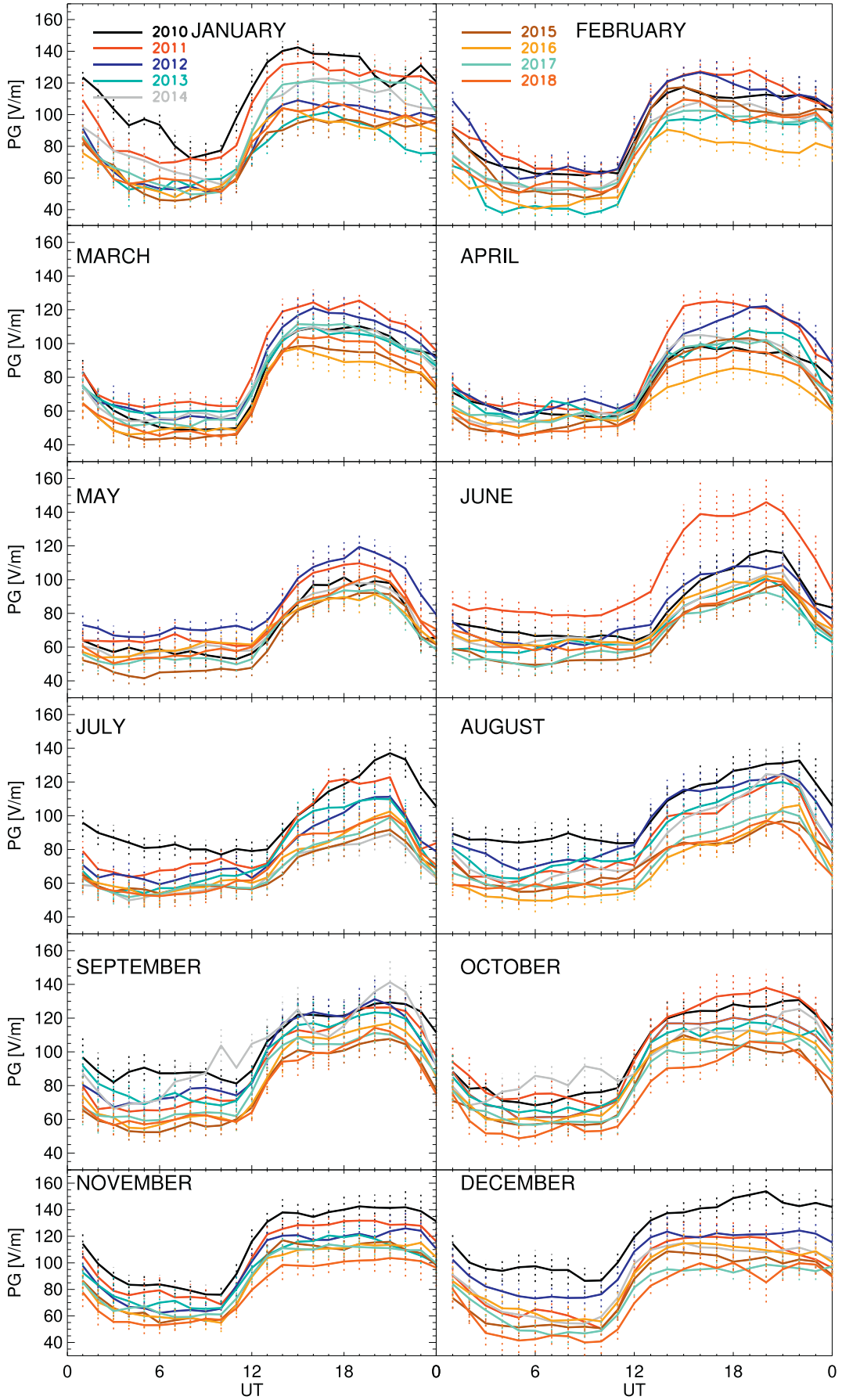

Fig. 2. PG standard curve for each month in 'fair weather' days (monthly standard curve), for nine years (2010–2018). The error bars represent one standard deviation.

Table 1
Number of 'fair-weather' days selected by month between January 2010 and December 2018.

Year	January	February	March	April	May	June	July	August	September	October	November	December
2010	3	17	19	20	13	15	18	10	13	10	18	10
2011	9	8	14	16	21	10	4	5	18	12	16	8
2012	8	6	21	18	21	8	15	12	20	17	15	21
2013	3	4	20	3	–	22	15	21	15	16	14	–
2014	9	13	21	26	24	16	15	17	3	3	–	11
2015	9	6	21	29	24	24	21	19	22	12	11	16
2016	13	18	21	16	28	25	20	20	23	14	17	22
2017	20	11	22	25	16	20	23	21	21	24	16	11
2018	10	10	21	23	20	23	22	26	21	17	18	5
Total	84	93	180	176	167	163	153	151	156	125	125	104

The dashed symbols '-' indicate no recorded data.

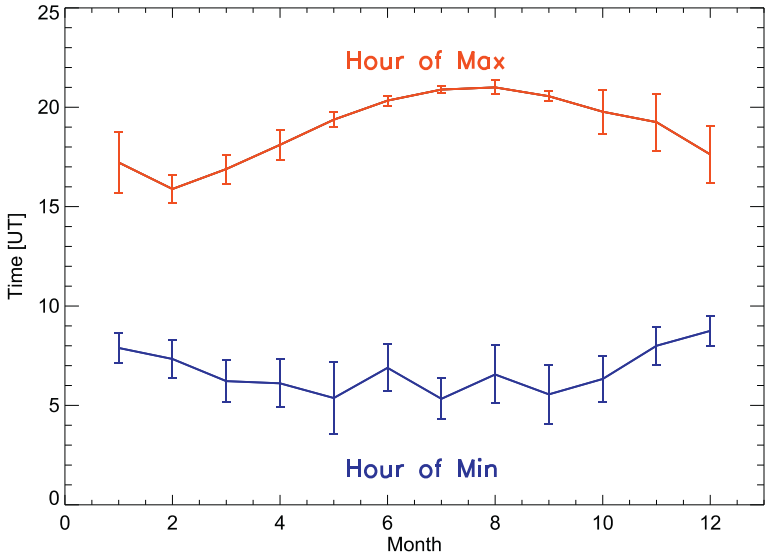

Fig. 3. Time of the maximum and minimum in the PG monthly standard curve, averaged for the period 2010–2018. The error bars represent 1σ mean values.

layer.[2] Furthermore, several studies show deviation of the PG values related to processes in the planetary boundary layer, such as production and transport of space charges, variation of the concentration of light ions, aerosols and in the radon emanation, resulting in changes in the electrical conductivity related to the development of convection (Israelsson and Tammet, 2001; Anisimov et al., 2012; Anisimov et al., 2014; Anisimov et al., 2017; Anisimov et al., 2018; Nicoll et al., 2018). These processes are more intense during summertime than wintertime producing high deviations in the PG when compared with the Carnegie curve (Israelsson and Tammet, 2001; Marcz and Harrison, 2003; Anisimov et al., 2014). Therefore, it should be also expected a better agreement during wintertime in the PG 'fair-weather' daily variation when comparing between different land stations far from anthropogenic pollution. This has recently been shown for different land stations in South America (Tacza et al., 2020). The correct identification of local effects on the PG in fair weather regions will be important in order to look for an overall variation of the global electric circuit.

In this study, we use nine years of PG data recorded at the CASLEO (Complejo AStronomico el LEOncito, Geographical coordinates: latitude: 31°47.88′S, longitude: 69°17.7′W, altitude: 2552 masl) since January 2010 until December 2018. CASLEO is an astronomical observatory located in the Andes Mountain of Argentina. This region is characterized by fair-weather conditions during almost the whole year. A detailed description of the site is explained in Tacza et al. (2018). In this work, we obtain the typical diurnal curve of the atmospheric electric field in fair weather conditions (standard curve) for CASLEO, which was compared with the 'universal' Carnegie curve. Additionally, we analyze the behavior of the PG seasonal variation with the occurrence of lightning and the atmospheric optical thickness. In Section 2 we presented the instrumentation and data analysis used in this work. The obtained results are divided in temporal (Section 3.1) and spectral analyses (Section 3.2). In Section 4 we discuss the differences and similarities between our standard curve and the Carnegie curve. Finally, the main results are summarized in the last section.

2. Instrumentation and data analysis

Potential Gradient (PG) measurements are continuously recorded at CASLEO (called CAS station) by an electric field mill (EFM) sensor. This station is part of a network of EFM sensors installed in South America (Tacza et al., 2014; Tacza et al., 2020) and a new global network to monitor the PG variation (Nicoll et al., 2019). The principle of operation of the EFM sensor is simple, when a conducting plate is exposed to

[2] Stull (1988) defined the planetary boundary layer as the lower part of the troposphere that is influenced by the presence of the surface of the Earth and respond to surface forcings, such as: frictional drag, evaporation and transpiration, heat transfer, pollutant emission and terrain induced flow modification. The thickness of the layer is quite variable in time and space, ranging from hundreds of meters to a few kilometers.

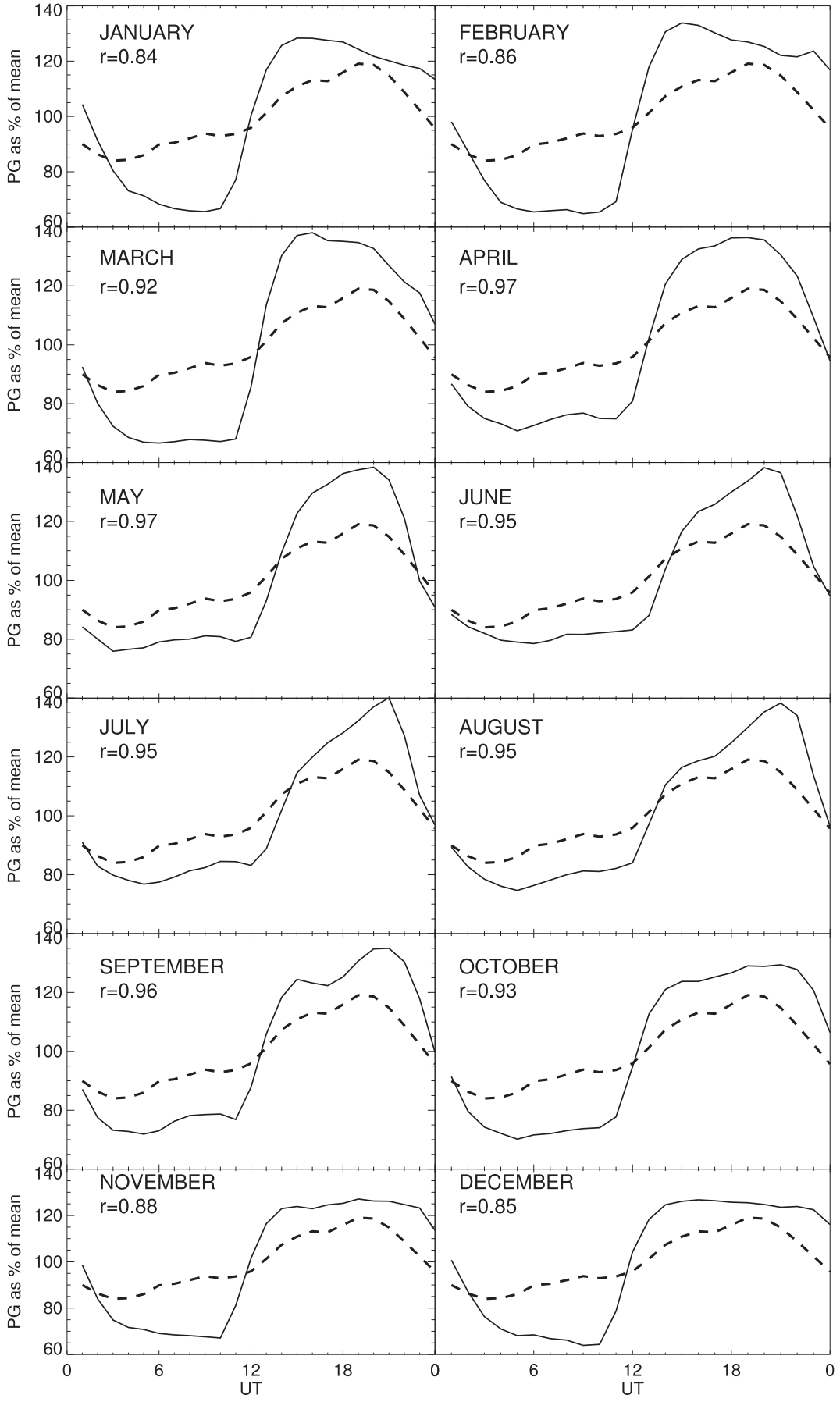

Fig. 4. PG monthly standard curve, averaged for the period 2010–2018, in 'fair weather' days (solid line) compared with the Carnegie curve (dashed line). The curves are plotted as a percent of the mean.

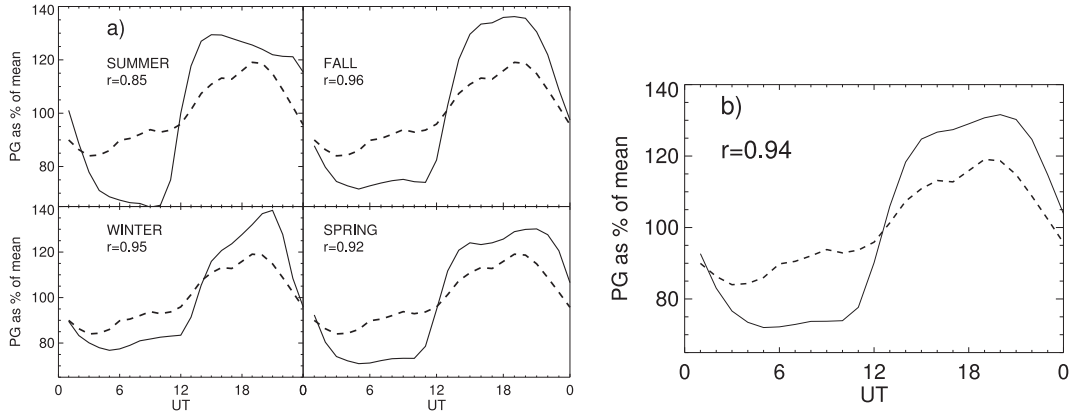

Fig. 5. (a) PG seasonal standard curve (solid line) compared with Carnegie Curve (dashed line) in terms of percentage from the mean. (b) PG annual standard curve (solid line) compared with Carnegie curve (dashed line) in terms of percentage from the mean.

an electric field, a charge is induced proportional to the electric field and area of the plate (Imyanitov, 1957; Secker, 1975). The time resolution of the EFM sensor is 0.5 s and for this work the records were integrated using a 60-min average. At CAS station, the EFM sensor is installed at a height of 1.5 m above the ground. This produce an overestimation of the electric field values, which were corrected for the reduction factor (Tacza et al., 2014; Tacza et al., 2020). Our analysis consisted of two steps: first, we obtain PG daily curve in fair weather conditions. For fair weather conditions, an observational criterion was chosen (Tacza et al., 2014; Tacza et al., 2020). This criterion considers days with PG values in the range 0–200 V/m. Once they are chosen, we calculated monthly, seasonal and annual averages of the PG variation called monthly, seasonal and annual standard curves, respectively. As second step, we compared our standard curves with the 'universal' Carnegie curve. Finally, a comparative analysis of the seasonal behavior of the PG measurements with the number of occurrences of lightning and the Aerosol optical depth (AOD) is performed.

For this last step, we used data of the STARNET and AERONET network. The STARNET network (Sferics Timing and Ranging Network) detects lightning by using Very Low Frequency (VLF) receivers (Morales and Anagnostou, 2003). The lightning propagates in the Earth-ionosphere waveguide and can be detected at very long distances. The time window of analysis used in this work is between January 2011 and December 2013. On the other hand, the AERONET (AERosol Robotic NETwork) program is a network of ground-based remote sensing photometers, which provides a continuous, long-term and easily accessible database for optical aerosol measurements, radiative and microphysical properties for aerosol searching among other applications. The network imposes instrument standardization, calibration, processing and distribution. The AERONET network utilizes the CIMEL multiband sun photometers (CE-318), which makes direct sun measurements on different spectral channels: 340, 380, 440, 500, 675, 870, 940 and 1020 nm (Holben et al., 1998). The network provides globally distributed observations of Aerosol Optical Depth (AOD), among other parameters. The AERONET network provides data at three levels of data quality: level 1 (raw measurements), level 1.5 (processed measurements, where cloud cover is removed) and level 2 (processed measurements and guaranteed by the network). In this work, we used AOD data for level 2 as an indirect measure of aerosol mass concentration. For this work, we used the AOD temporal variation from an AERONET network station located at CASLEO (~300 m away from CAS sensor) since January 2011 until July 2014 when the data was available.

In addition to the temporal series analyses, we performed a spectrum analysis for all PG data using the wavelet technique. The wavelet analysis is described further in Section 3.2.

3. Results

Fig. 1 shows the histogram for all PG hourly values for the period January 2010–December 2018. The PG mean value is 78.8 V/m and the median value is 79.1 V/m. If only 'fair-weather' days are considered, the PG mean value is 82 V/m and the median value is 79.3 V/m.

3.1. Time series analysis

3.1.1. Diurnal variation

Fig. 2 shows the PG monthly standard curve for nine years between January 2010 and December 2018. The error bar represents 1σ (one standard deviation). Two things are significant: first, the shape of the PG monthly standard curve is almost the same for the different years, especially during winter months in the South Hemisphere (with exception of July 2010 and June 2011) and, second, a clearly decrease of the PG amplitude is observed until 2015. As expected, these features are similar for the seasonal and annual standard curves (not showed here) and will be discussed further in the next section. Table 1 gives the number of 'fair-weather' days selected for each month. It is clear that there is more 'fair-weather' days during months between March and November than during summer time in the South Hemisphere (December, January and February). This is because during summer, several days are affected by disturbed weather (e.g., thunderstorm) occurring near the sensor location.

Fig. 3 shows the averages of the maximum and minimum time for each PG monthly standard curve. During wintertime (June, July and August) the maximum and minimum time are at 20 UT and 6 UT, respectively, while those during summertime (December, January and February) occurs at 15–16 UT and 8–9 UT, respectively.

Fig. 4 shows the comparison between the PG monthly standard curves, averaged for all years, and the 'universal' Carnegie curve (Harrison, 2013), plotted as percent of the mean. The same is shown in Fig. 5 but for the PG seasonal and annual standard curves. Two facts are significant from Figs. 4 and 5: first, the amplitude variation of the

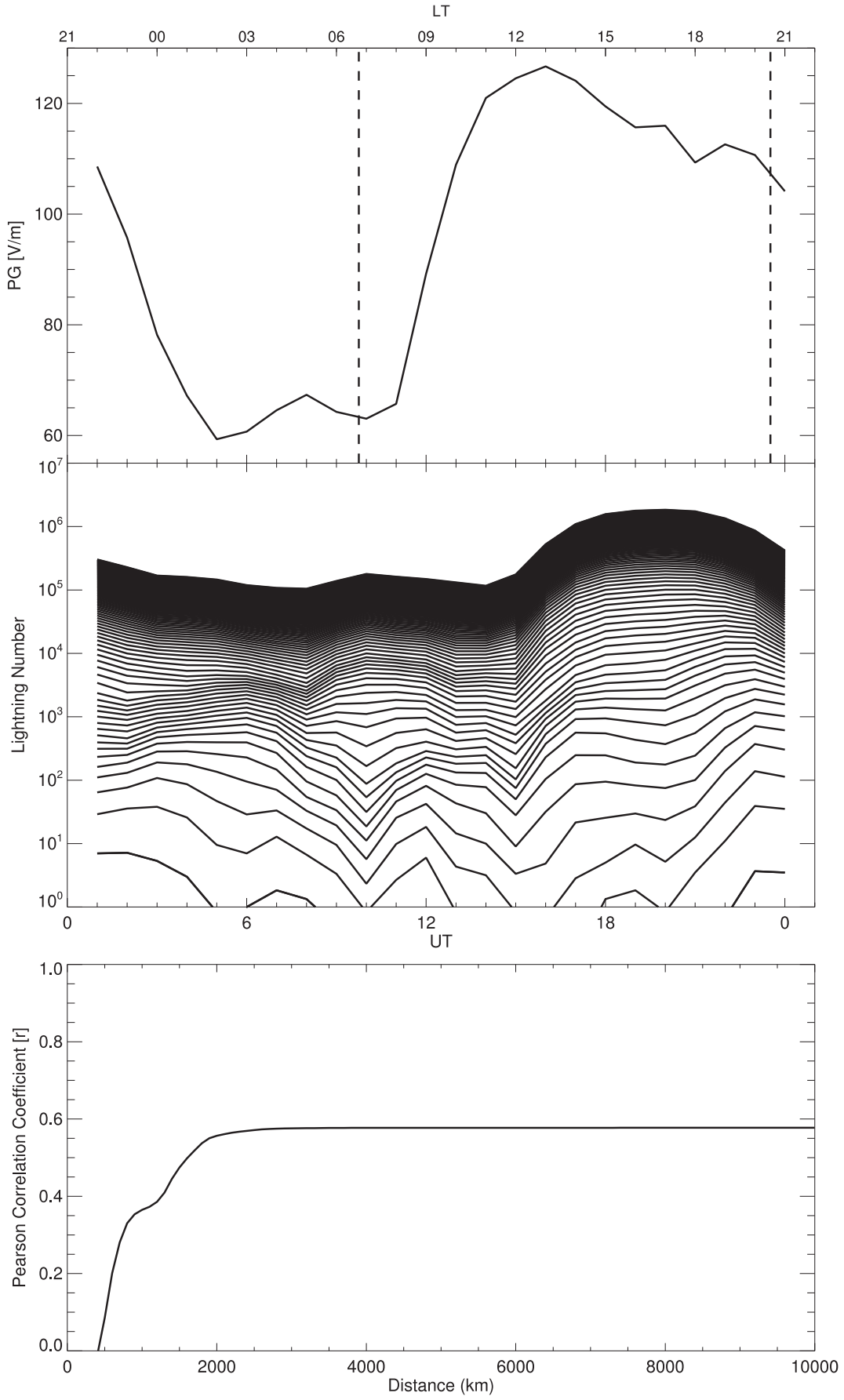

(caption on next page)

Fig. 6. PG monthly standard curve for February 2012 (top). Monthly average daily variation in the number of lightning occurrences for February 2012 for distances between 0 and 10,000 km (middle). Pearson correlation coefficient between the PG and number of lightning curves for each distance (bottom). Vertical dashed lines indicate the sunrise and sunset times, respectively.

standard curve is almost twice the Carnegie curve and, second, the Pearson correlation coefficient is lower for summertime than wintertime. Then, the shape of the standard curve is more similar with the Carnegie curve during wintertime. This is also in agreement with Fig. 3, where it is observed that the maximum and minimum times, for CAS station, in winter are at 20UT and 6UT, respectively. These values are closer to the maximum and minimum times of the Carnegie curve (19UT and 3UT, respectively). In Fig. 5, we note high correlations between our standard curves (seasonal and annual) and the Carnegie curve, with values higher than 0.92, except for the summer curve (0.85). In addition, the amplitude variation for the Carnegie curve is 35%, while for our standard curves are 59% (annual), 68% (summer), 62% (fall), 59% (winter) and 59% (spring). This difference in the amplitude variation can be due to local effects (e.g. aerosol concentration) in our measurements. Although, CAS station is located far from the city, and therefore there is little anthropogenic pollution, there is still the presence of a background of natural aerosol (e.g., dust, etc.).

As mentioned in the introduction section, the PG in fair weather is mainly generated by atmospheric electrical activity occurring in remote disturbed regions. Therefore, a good correlation between both parameters is expected in fair weather days. In order to compare our standard curves with electrical activity, we calculated the correlation between the PG standard curve and electric storms activity. To get an estimate of the thunderstorm number, we used the number of lightning occurrences recorded by the STARNET network. The number of lightning was calculated for distances ranging from 0 to 10,000 km away from CASLEO observatory.

Figs. 6 and 7 show (upper panel) the PG monthly standard curve for February and July 2012, respectively. The middle panels show the mean monthly lightning number for distances from 0 to 10,000 km. The mean monthly lightning number was calculated using the same days as the PG monthly standard curve. Note that when the distance increases, the number of lightning increases and the shape of the curve is more similar with the PG monthly standard curve. The lower panels of Figs. 6 and 7 show the Pearson correlation coefficient, r, between the standard curve and the lightning number curve for each of the distances. Fig. 6 shows that r increases as the distance increases. From distances of 2000 km and above, r reaches its maximum value ($r \sim 0.6$) and then remains constant. Similar behavior is observed in Fig. 7 with r reaching its maximum value at about 4000 km ($r \sim 0.8$). The reason why r reaches a maximum at different distances can be understood in terms of the occurrences of electric storms. February is summertime for South America and the electric storms occurs closer to CASLEO observatory, but July, is wintertime and storms occurs farther. Additionally, from the middle panels of Figs. 6 and 7, is observed that the number of lightning is higher in summer than winter. The values of $r = 0.6$, for February, and $r = 0.8$, for July, mean that in wintertime a higher correlation is obtained between the monthly lightning number and the PG monthly standard curve when compared with that of summertime. In addition, it is important to note that the February PG monthly standard curve has a bump between 10 and 13 LT, different from the Carnegie curve. However, for the July PG standard curve this bump disappears, and the shape of the standard curve is more like the Carnegie curve. This bump is observed after sunrise and can be produced by the effects of turbulence and/or convection of the Earth's surface. This will be discussed further in the next section.

Fig. 8 shows the r values calculated for each month of 2012 employing the same methodology described for Figs. 6 and 7. The r values are lower during summertime compared with those of the other seasons. This finding may arise the hypothesis that convective effects, which are more important in summer, perturb more the PG standard curve during summer than winter.

On the other hand, in order to estimate the aerosol concentration daily variation, the AOD variation was analyzed. Figs. 9 and 10 show the comparison between daily average variations of PG, AOD at different wavelengths (AOD_1020nm for a wavelength of 1020 nm and so on) and meteorological parameters (temperature, relative humidity and wind speed). The daily variations were computed for 50 summer (DJF) days and 77 winter (JJA) days, respectively, between January 2011 and July 2014. The Carnegie curve (blue dotted line) is shown for comparison in the top panel. AOD is recorded only during daytime. The meteorological parameters were recorded by a meteorological station installed 1.5 km away from CASLEO observatory. The figures show that the PG mean daily amplitude is greater in summer (95 V/m) than in winter (79 V/m). Similarly, the AOD amplitude is greater in summer that in winter for all wavelengths (for example AOD_380nm is 0.047 in summer and 0.021 in winter).

Fig. 9 shows a clear difference between the CASLEO PG daily variation and the Carnegie curve (in agreement with Fig. 5a). The AOD values start to decrease after the sunrise reaching a minimum around 17–18 UT (14–15 LT). After that, AOD values start to increase. This behavior is observed for all wavelengths. The meteorological parameters also follow a daily variation: the air temperature values start to increase after the sunrise and is anticorrelated with the relative humidity. Wind speed values are less than 5 m/s during most part of the day (except during 00–02 UT and 21–24 UT when the values are between 5 and 8 m/s). On the other hand, Fig. 10 shows a similar behavior between the PG daily variation and the Carnegie curve. The AOD daily variation is not clear anymore. The air temperature and relative humidity still present a daily variation but less intense. Wind speed values are less than 5 m/s during all day.

As is observed from Figs. 4 and 5, the amplitude variation for Carnegie curve is around 35%, which was also found for thunderstorm and electric shower clouds activity (Peterson et al., 2017). Taking this into account, we selected manually by eye inspection only days with this similar amplitude variation. From 1672 days (between 2010 and 2018), this characteristic was observed in 162 days. This number is about only 10% of the total days we catalogued as 'fair weather' days. The result is shown in Fig. 11, where the PG standard curve, mean (black line) and median (blue line) curve, are compared with the Carnegie curve (red line). There is a clear similarity in the shape between the curves. The correlation coefficient between both curves is $r = 0.98$. The maximum and minimum time are almost the same, 19–20 UT and 3–4 UT, respectively. From these 162 days, 105 days were found in the period May–September and 57 days in the period October–April. Evidently, an analysis of the meteorological conditions for these particular days with the PG amplitude variation like Carnegie curve deserves a further study.

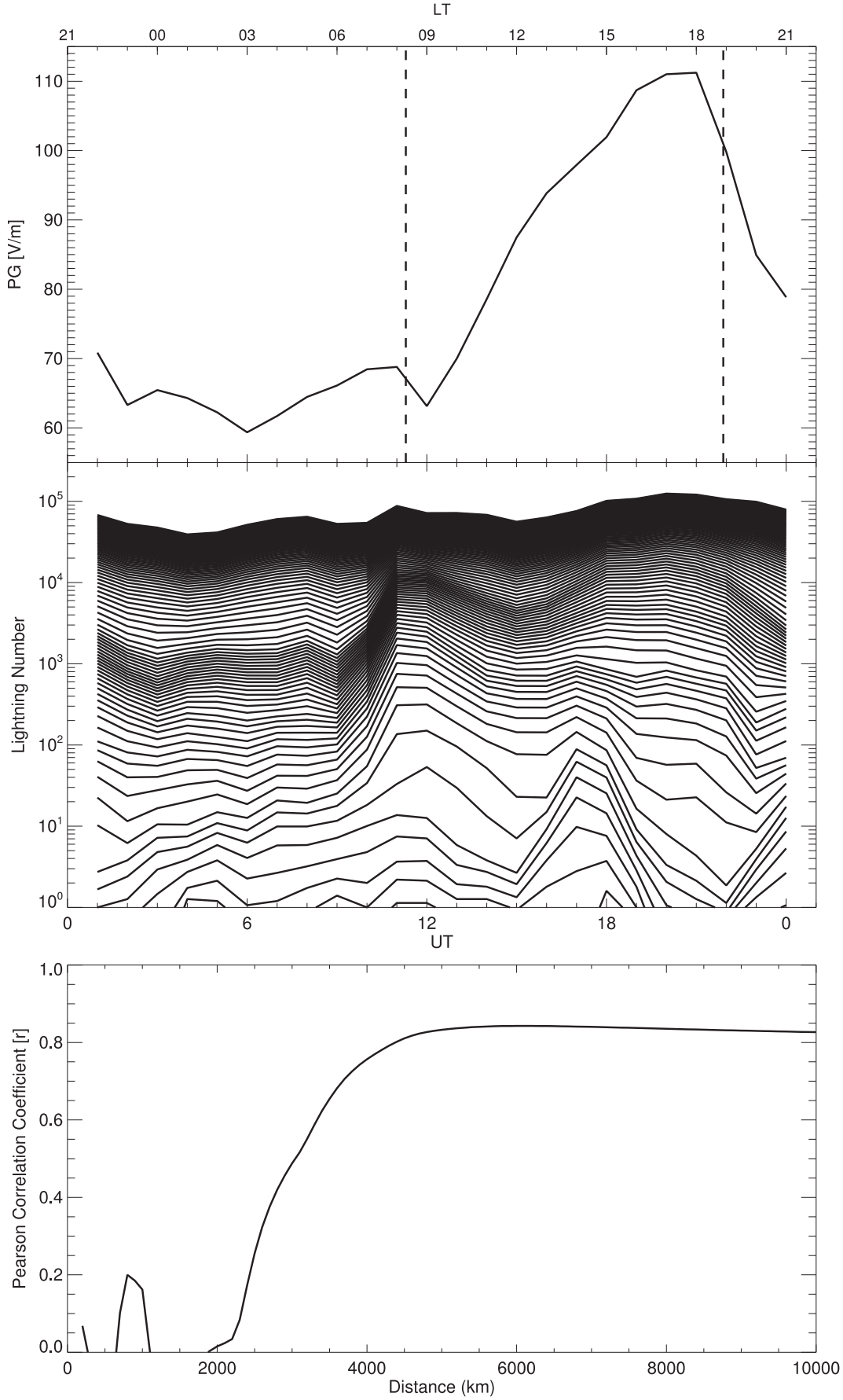

Fig. 7. As in Fig. 6 but for July 2012.

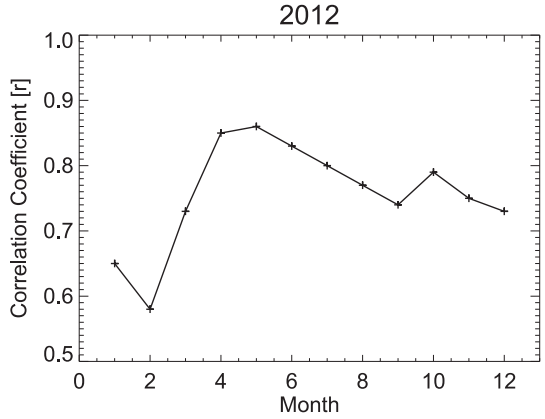

Fig. 8. Pearson correlation coefficient between the PG monthly standard curve and the monthly average daily variation in the number of lightning occurrences, for distances ≥3000 km.

3.1.2. Seasonal variation

In addition to the diurnal variation, we analyzed the behavior of the seasonal variation of the PG values for CAS station. Fig. 12 shows the entire time series of PG daily averages for 'fair-weather' days from January 2010 to December 2018. At the top is the daily average between 00 and 24 UT, the second panel shows the average for 00–08 UT, the third panel shows the average between 08 and 16 UT and the lower part for the 16–24 UT. The red curve is a 31-day simple moving average. The vertical red dashed lines indicate the beginning of each year. A seasonal variation with high PG values is observed during November–January and low values during April–June, for the four time windows (00–24, 00–08, 08–16 and 16–24 UT).

Fig. 13 shows the average value of the monthly standard curves. This figure confirms for each year that the PG amplitude has high values during November–January and low values during April–June. This seasonal variation is almost opposite to the seasonal variation of electrical activity (Christian et al., 2003). As discussed by Adlerman and Williams (1996), influence of aerosols can obscure a global variation in the atmospheric electric field. Figs. 9 and 10 show that AOD is greater in summer than in winter, therefore, an effect of aerosol on the seasonal variation should be considered.

To analyze the influence of aerosols on the long-term atmospheric electric field, we compared the measurements recorded at CASLEO by the AERONET and AFINSA networks. The data period available for AERONET is from January 2011 to July 2014, thus, we used the CAS PG data for the same period. Fig. 14 shows the monthly average variation of AOD for different wavelengths. The AOD variation is compared with the mean value of the PG monthly standard curves (dashed black curve). There is a similarity in the seasonal variation for the AOD and PG values, which is low values between May–July and high values between December–January. This is more evident when comparing PG values with AOD of shorter wavelengths. This seasonal variation is opposite to the global seasonal variation of electrical activity, which may indicate that aerosols are obscuring a global effect on the seasonal variation of the electric field as previously mentioned. In this subsection, we try to remove the influence of aerosols on the PG values in 'fair-weather' days.

For a more detailed analysis between the PG and the AOD, a simple linear correlation was calculated between both variables taking into account fair weather conditions. In order to do that, a meteorological station 1.5 km away from CASLEO was used. The PG and AOD values were correlated on days without rain and with wind speed less than 8 m/s. Fig. 15 shows the daily averages of PG versus AOD values for the different wavelengths (a) and only for the 500 nm wavelength (b), as well as the respective Pearson linear correlation coefficients, r, between both variables. The values of the linear correlation coefficient are greater than 0.5 for all wavelengths.

The relation in Fig. 15 suggests that $PG_T = PG_A + PG_0$, where PG_T is the total PG, PG_A is the PG influenced by aerosols and PG_0 is the PG in fair weather. PG_A can be expressed as $PG_A = kAOD$, where k is a constant and we assume AOD is linearly dependent of the aerosol mass concentration. This last statement is supported by several studies (Smirnov et al., 2000; Wang and Christopher, 2003; Gupta and Christopher, 2008; Boyouk et al., 2010). Fig. 15b shows the linear correlation between PG and AOD values for the 500 nm wavelength with their respective linear fitting (red line). We found for PG free of aerosol $PG_0 = 82.7 V/m$. The same procedure was performed for each wavelength. Fig. 16 shows the average monthly variation of PG after removing the influence of aerosols for each wavelength (dashed line). The solid line is the same variation after applying a 3-month simple moving average. Vertical lines indicate the beginning of each year.

To compare the seasonal variation between the PG values, after removing aerosol influence, and the electrical activity, occurrence of lightning number recorded by the STARNET network was used. The data available was between January 2011 and December 2013. Fig. 17 shows this comparison between the monthly average variation for the number of lightning (blue curve, with a 3-month simple moving average detected for a distance between 3000 and 18,000 km away from CAS station) and the monthly average variation of the PG in 'fair-weather' (black curve, 3-month simple moving average). For comparison purposes, both curves were normalized to their maximum value. We observe a general agreement for short wavelengths. This is especially true for years 2012 and 2013. The results show that after correcting the PG values by the influence of aerosols (AOD) a similarity is observed between the seasonal variation of the PG and the electrical storms occurrences. This fact supports the initial hypothesis that aerosols may obscure the global effect of the electrical activity over the PG variation, as already mentioned by other authors (Adlerman and Williams, 1996). In particular, similar seasonal variation between the PG and the electrical activity is more significant for shorter wavelengths (e.g., for 380 nm we found $r = 0.7$). Whether exist a relationship of PG with the size of the aerosol particles is currently beyond the scope of this paper. However, we agree that this is a subject that is worth investigating as a follow up study.

3.2. Spectral analysis

In this section, the continuous wavelet transform (Torrence and Compo, 1998) is employed to retrieve the important oscillations appearing in the PG variability. The analysis was performed similarly as described by Macotela et al. (2019). Essentially, the continuous wavelet transform toolbox for MATLAB package provided by Grinsted et al. (2004) is used. We also employed a Morlet mother function with frequency $w_0 = 7$ and 8 sub octaves per octave (8 voices per power of two). Considering that for geophysical time series a red-noise assumption is often suitable (Grinsted et al., 2004). We estimated the red-noise background using the lag-1 and lag-2 autocorrelations of the PG hourly amplitudes. This autoregressive value is 0.9. Fig. 18a shows the time series for the PG hourly amplitudes since January 2010 until December 2018 for fair weather days. In this figure, the occasional data gaps

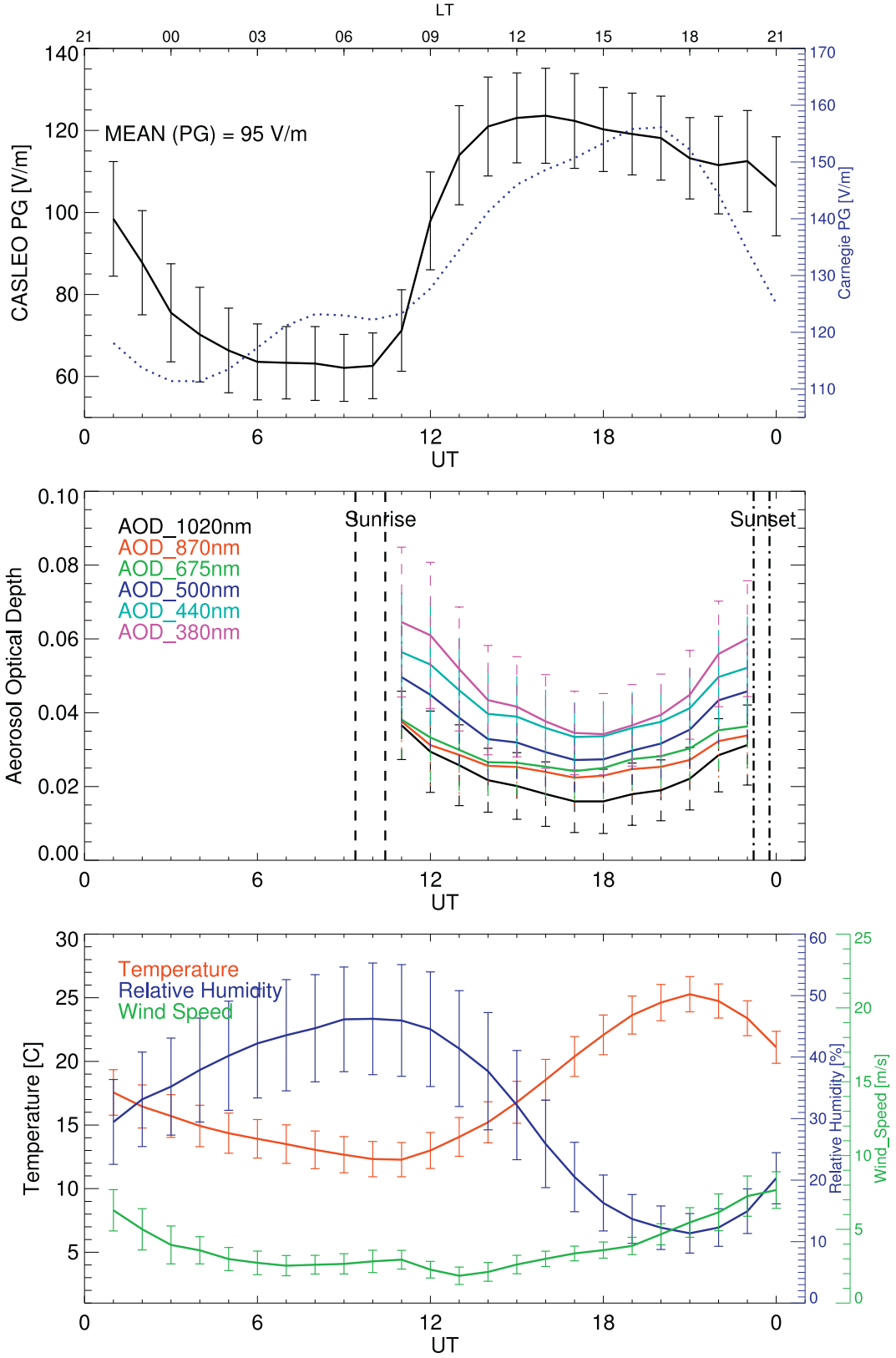

Fig. 9. PG (top), aerosol optical depth (middle) and meteorological parameters (bottom) daily variation for the mean of 50 summer days (DJF) between 2011 and 2014. Vertical lines in the middle panel indicate the sunrise and sunset period during summer (DJF), respectively. The error bars represent one standard deviation.

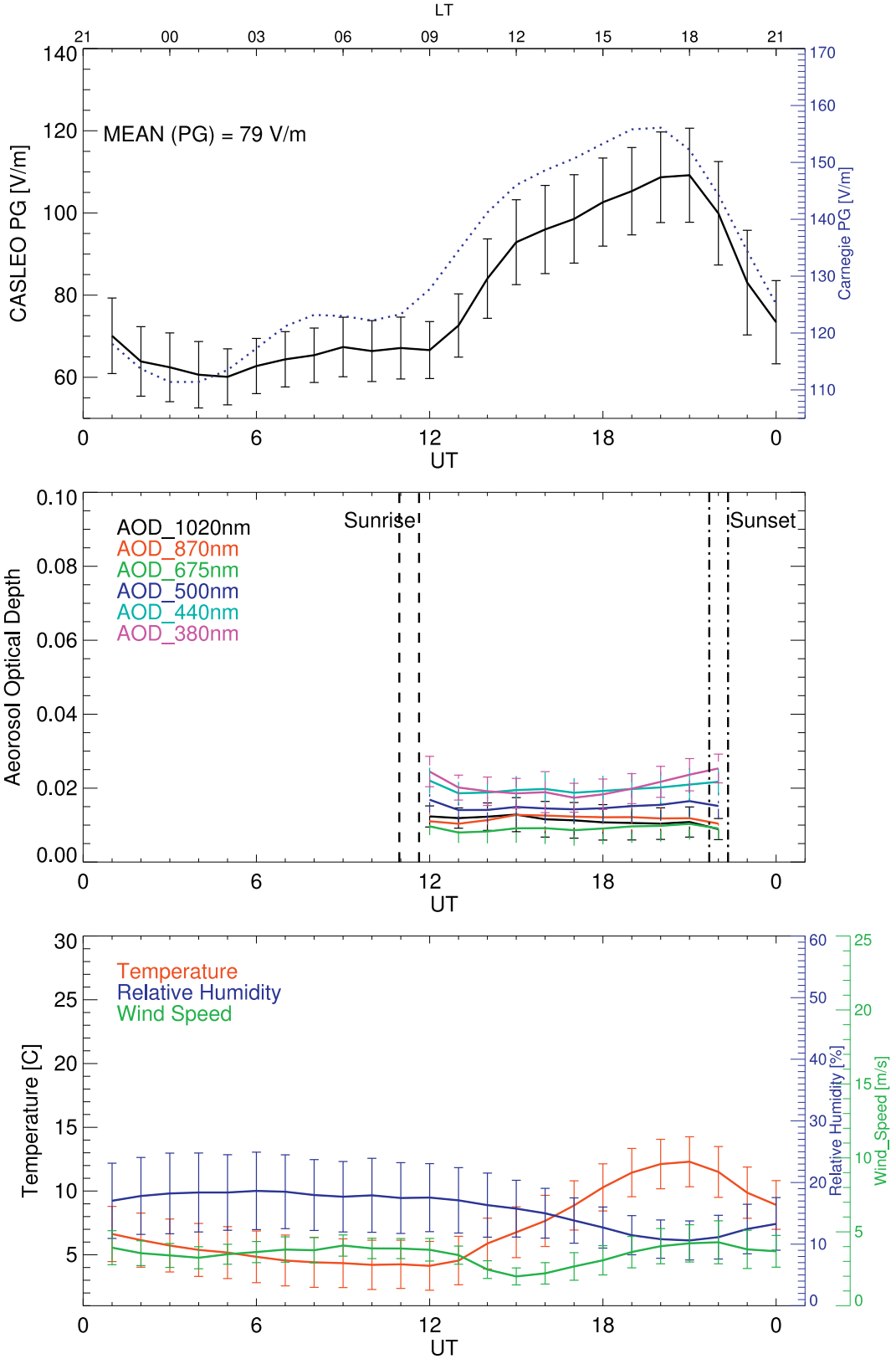

Fig. 10. As in Fig. 9 but for the mean of 77 winter (JJA) days between 2011 and 2014.

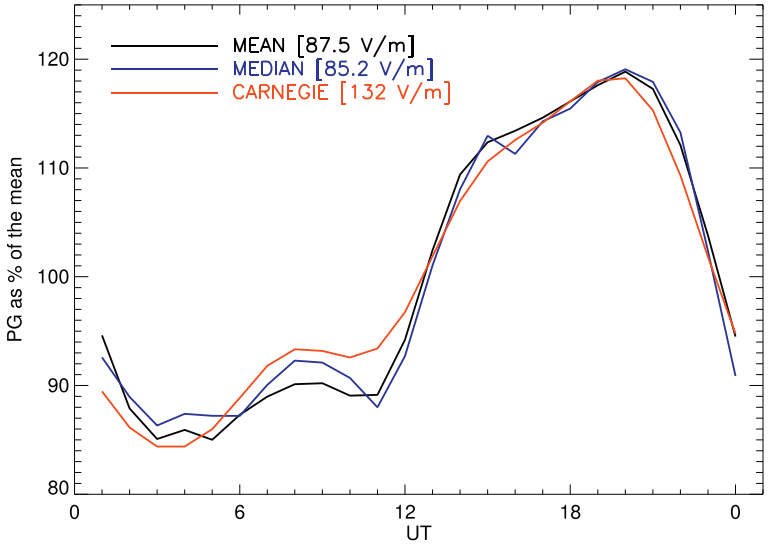

Fig. 11. Mean (black) and median (blue) values of the PG diurnal variation for 162 days selected by eye (like Carnegie shape) compared with the Carnegie curve (red line). The three curves are plotted as a percent of the mean.

correspond to periods of power supply interruption. To apply the wavelet analysis, constant time steps between samples is demanded. Thus, those gaps were filled by using its respective smoothed value, which is obtained by applying a moving average with a time window length of 1419 h to the original time series. As stated by Macotela et al. (2019), this procedure minimizes the introduction of artifacts in the wavelet analysis.

Fig. 18b shows the global wavelet power spectrum, i.e., the time averaged wavelet power spectrum, where each period was corrected by its scale. This correction is employed to rectify the wavelet spectrum, which is biased in favor of larger periods (Liu et al., 2007). The dashed line is the 95% confidence level of the global wavelet power spectrum for its autoregressive value of 0.9. Powers above this line are regarded as significant, which maxima are indicated by horizontal lines. The corresponding significant periods are identified as 1-, 165- and 361-day. Fig. 18c shows the real part of the wavelet transform corrected by the scale. The contours represent the magnitude of the matches between the phases of the time series and the wavelet. The color bar indicates the amplitude of those contours that changes from white to red. The horizontal lines identify the significant periods and the black curve is the cone of influence. The values below this curve must be evaluated with discretion. In Fig. 18c, 1- and 361-day oscillations can be clearly seen for all the analyzed years, where the 1-day oscillation amplitude is stronger than the one corresponding to the 361-day oscillation. Interestingly, a 165-day oscillation appears with noticeably weaker amplitude than the previous two oscillations. However, this oscillation is not well defined around 2012–2014 and from 2015 onwards.

From Fig. 18b and c, the 361-day period can be interpreted as an annual oscillation (AO), and the 1-day period as the diurnal oscillation. In general, Fig. 18 shows that the important oscillations undergo changes in amplitude with time or even completely vanish only to reappear some time later.

4. Discussions

The present study shows an analysis on the Potential Gradient (PG) variability recorded at CASLEO observatory (Argentina) during nine years (2010–2018). We have estimated monthly, seasonal and annual averages of the PG diurnal variation in 'fair-weather' conditions, which we called as monthly, seasonal and annual standard curve, respectively. Our analysis shows that the diurnal variation of the monthly standard curve is preserved each year, revealing the high reliability of our measurements (Fig. 2).

Our findings demonstrate a high Pearson linear correlation (r = 0.85–0.95) between the standard curve and the 'classic' Carnegie curve (Figs. 4 and 5) and the features of the seasonal and annual standard curves are quite the same. Therefore, our discussion focusses mainly on the evaluation between our standard curves with the Carnegie curve. First, the Carnegie curve has a minimum and maximum time at 3 UT and 19 UT, respectively, and shows three peaks at 8, 14 and 19 UT, associated to the electric activity worldwide (Asia/Australia, Africa/Europe and America, respectively). Taking into account that the Carnegie curve was calculated using an average of 82 days, the minimum and maximum times must be taking with precaution. A reanalysis of the PG measurements over the oceans reported by Harrison (2013) shows that the minimum time varies between 2 and 5 UT and the maximum time between 17 and 22 UT throughout the year. In our case, the monthly standard curve has a minimum time ranging between 5 and 8 UT and a maximum time ranging between 16 and 21 UT (Fig. 3). In particular, these times are more comparable with those of the Carnegie curve during wintertime (JJA) than during summertime (DJF) for the Southern Hemisphere. Furthermore, the three peaks observed in the Carnegie curve (~ 8, 14 and 19 UT) are also observed in the monthly and seasonal standard curve (Figs. 4 and 5, respectively). However, the matching in time is more clearly observed during wintertime than during summertime. In particular, the peak that occurs around 8 UT (Asia/Australia peak) is not clearly observed during summertime. In addition, the standard curve suffers significant displacement of its maximum time to early hours. In other words, the maximum peak expected at 19 UT is observed at 14–15 UT in summertime.

With respect to the amplitude variation, the Carnegie curve has an amplitude variation of ~35%, which was also found in the electric activity worldwide (Peterson et al., 2017). However, amplitude of the

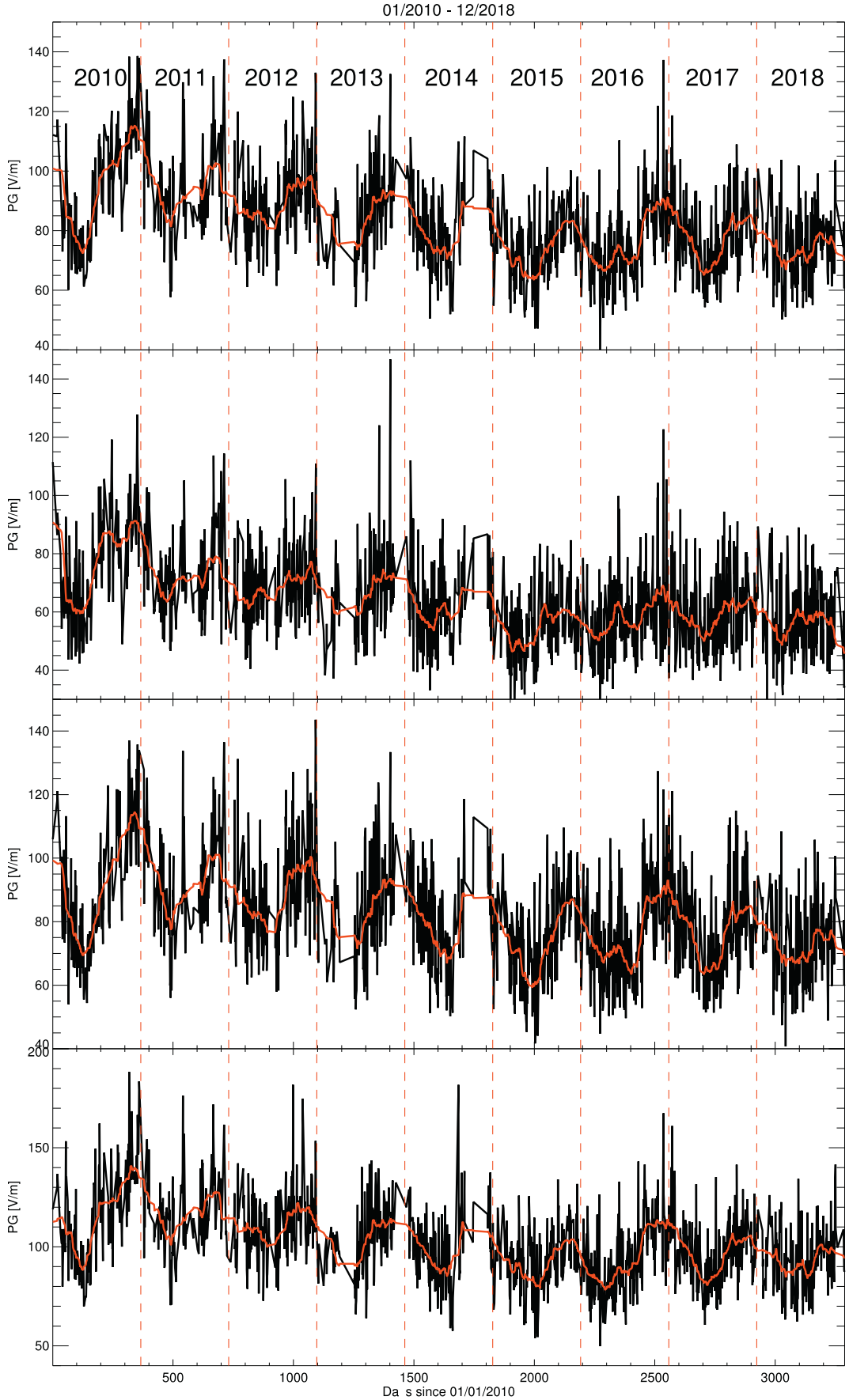

Fig. 12. PG daily variation for fair weather days (top: average for 00–24 UT, second panel: average for 00–08 UT, third panel: average for 08–16 UT and bottom: 16–24 UT) for the period from 1 January 2010 to 31 December 2018. The red curve is a moving average of 31 days. Vertical dashed red lines indicate the beginning of each year.

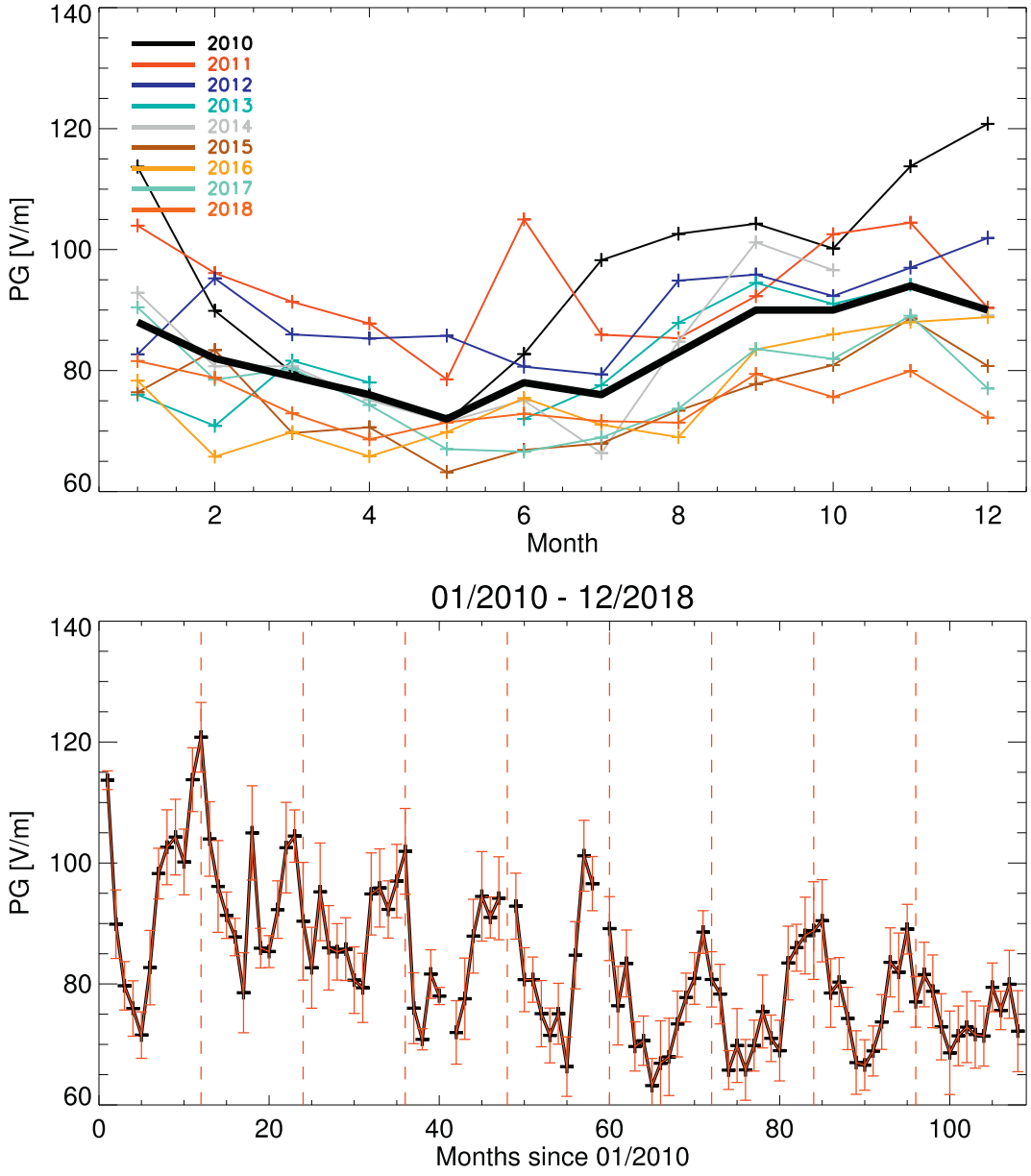

Fig. 13. PG monthly mean variation for fair weather days for the period January 2010 to December 2018 where the thick black line represents the mean value for each month (top). Time series of PG monthly averages for the same period (bottom). Vertical dashed red lines indicate the beginning of each year. The error bars are 1σ.

annual standard curve for CAS is almost twice. Furthermore, this amplitude is greater in summer (~65%) than in winter (~58%). Regarding the Pearson linear correlation coefficient between the seasonal standard curve and the Carnegie curve, this value is lower in summer (r = 0.85) than in winter (r = 0.95). In summary, our standard curve shows a better agreement with the Carnegie curve during wintertime (JJA) than during summertime (DJF). We would like to point out that similar correlation coefficients were expected for every season. Interestingly, this difference indicates us that there is another phenomena taking place during summer time that influence the PG values.

An additional analysis employing our monthly standard curves and the monthly electrical activity worldwide results in a better linear correlation coefficient for wintertime (r ~ 0.8) than summertime (r ~ 0.65), as shown in Figs. 6, 7 and 8. Therefore, these results confirm our previous finding that the PG standard curve for CAS station shows a better agreement with the electric activity variation in wintertime.

In order to understand why the PG standard curve differs more in summer than winter at CASLEO, the influence of local effects was considered. Taking into account that the nearest city is ~40 km away, the influence of anthropogenic pollution can be discarded. Nevertheless, CAS station is susceptible to be influenced by non-anthropogenic effect, such as the sunrise effect, the 'Austausch' generator

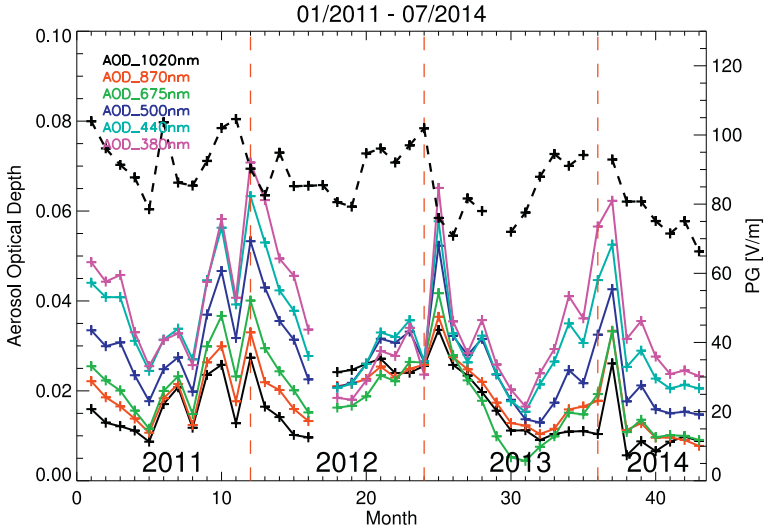

Fig. 14. Monthly values of aerosol optical depth for different wavelengths (colors line) and monthly values of potential gradient (dashed thick line).

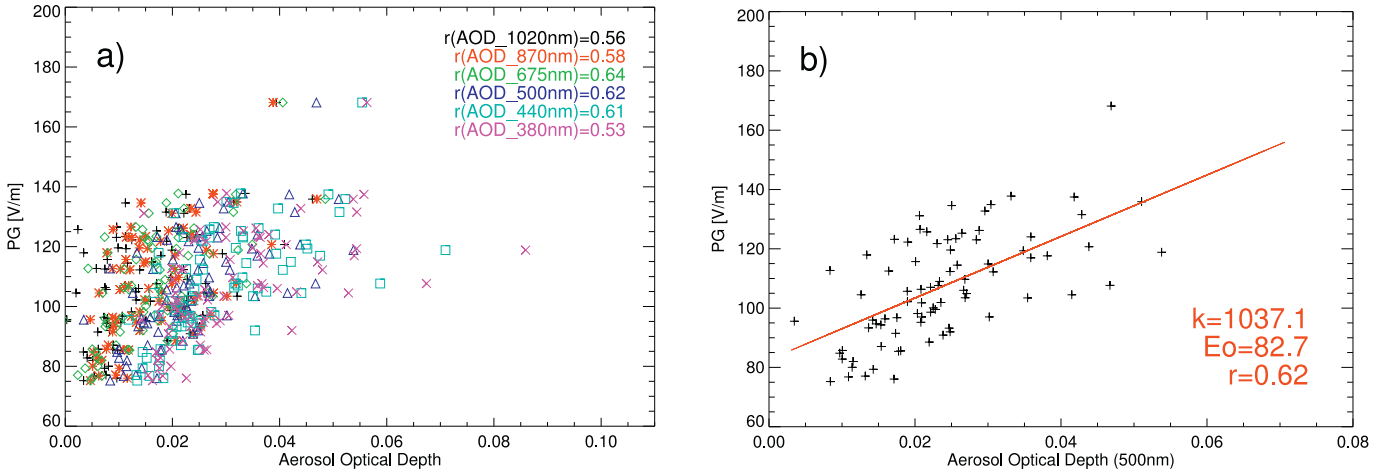

Fig. 15. (a) PG values versus AOD for fair weather conditions for different wavelength. (b) Linear correlation between PG values and AOD (500 nm).

and processes associated to the development of the planetary boundary layer. A simple mechanism to explain our results could be associated to a reduction of the electrical conductivity as proposed by Anisimov et al. (2018). After the sunrise, the temperature starts to increase producing convection/turbulence upward, which dissipate radioactive gases at the ground (e.g., radon and its radioactive decay products through attachment with aerosols) and, therefore, the electrical conductivity at the ground decreases and the PG increases. The daily variation in the aerosol load (AOD) could give an idea of the development of convection/turbulence, which AOD values start to decrease after the sunrise due to the mixing/dissipation of aerosols in the planetary boundary layer. By contrast, in wintertime all these processes are less intense producing little changes in the PG (Fig. 10). It is important to note that although there is no similar daily variation between PG and AOD in both seasons (Figs. 9 and 10) the aerosol load in summer is higher than in winter, which can intensify the processes previously mentioned.

We have suggested that the convective process is the main effect producing the deviations in phase and amplitude when the PG standard curve and the Carnegie curve are compared, and, its influence is more significant in summertime (DJF). Nevertheless, we found few days (162 from 1672 days) for which the PG measurements for CAS station met the same features as the Carnegie curve (i.e., phase and amplitude). This comparison is shown in Fig. 11. Our standard curve and the Carnegie curve are very similar ($r = 0.98$) in phase and amplitude variation. Analysis of the meteorological features for these 162 days is out of the scope of the present study and is going to be addressed in a future study.

It is important to highlight that local effects produced by convective process in the PG variation are present continuously every day and therefore they appear in the monthly, seasonal and annual standard curves. Daily disturbances in the PG values associated with external geophysical phenomena can be observed by performing the simple difference between the PG values, measured on the day of the phenomena, and its monthly, seasonal or annual standard curve as shown in Tacza et al. (2016) and Tacza et al. (2018).

CASLEO station is almost free of anthropogenic pollution and has

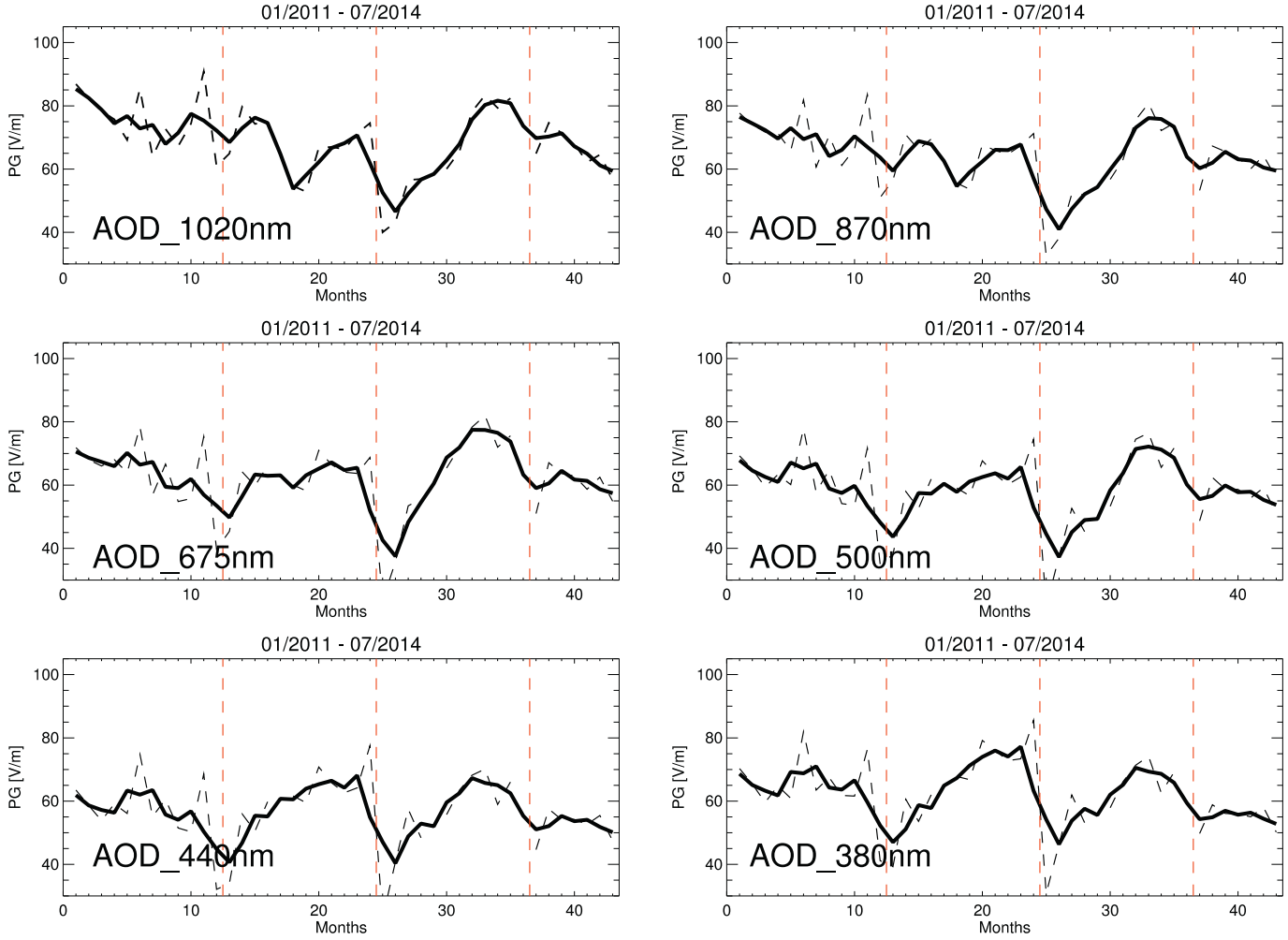

Fig. 16. Average monthly of the PG corrected by the influence of aerosols (dashed line) for each wavelength. The continuous solid line is a 3 month moving average.

been listed as a low-aerosol load site in the world (Martins et al., 2017). However, it still presents a seasonal variation (Fig. 14) possibly related to the transport of biomass burning in the Amazonian and mineral dust (Videla et al., 2013; Martins et al., 2017). Similar behavior in the aerosol seasonal variation was found for near places, such as Tucuman (Garcia et al., 2018) and Cordoba (Ceca et al., 2018) in the north of Argentina. Thus, influence of aerosols on the PG seasonal variation should also be expected. From report of Christian et al. (2003), we understand that the seasonal electrical activity variation has maximum values during wintertime (JJA) than during summertime (DJF) for the Southern Hemisphere. This seasonal variation was also found by a re-analysis of PG measurements performed by the Carnegie cruises (Adlerman and Williams, 1996) which is in accordance to the global electric circuit model. Furthermore, the same seasonal variation was found for the PG variation recorded in the Antarctica (Burns et al., 2012; Jeeva et al., 2016). However, PG measurements in land continent can suffer aerosol influence, which obscure a global effect on the PG measurements (Adlerman and Williams, 1996). From Figs. 12 and 13 and from the well-known seasonal electrical activity variation we can infer that the PG seasonal variation for CAS station is opposite to the seasonal variation of the electrical activity. This opposed behavior can be explained by the fact that aerosols obscure global effects on the PG seasonal variation as previously mentioned. The similar behavior observed between PG and AOD parameters (Fig. 14) supports our previous finding of the PG seasonal variation dependence on aerosol amount. After removing the influence of the aerosols on the PG values (Figs. 15 and 16) we found a better correspondence between the PG variation and the electrical activity (Fig. 17), especially for short wavelengths. This result is in support of previous hypothesis that aerosols obscure a global effect of electrical activity on the PG variation in fair weather regions.

On the other hand, there is a clear decrease of 330 mV/m per month in the PG amplitude values for CAS station for the period January 2010 to December 2015. After that, the decrease is no longer present and the PG values have remained stable until December 2018. Long-term changes in the PG values may be due to three factors: EFM sensor failure, local effect (e.g., variation in aerosol concentration) or global effect (e.g., changes associated to the solar activity cycle). The instrumental failure may be due to physical deterioration in the mechanical part of the sensor affecting the sensitivity of the measure. However, if it was an instrumental problem the amplitude values should have continuously decreased until December 2018. Therefore, an instrumental failure can be excluded. A possible change in aerosol concentration at the measurement site may also disturb the PG. Unfortunately, there is

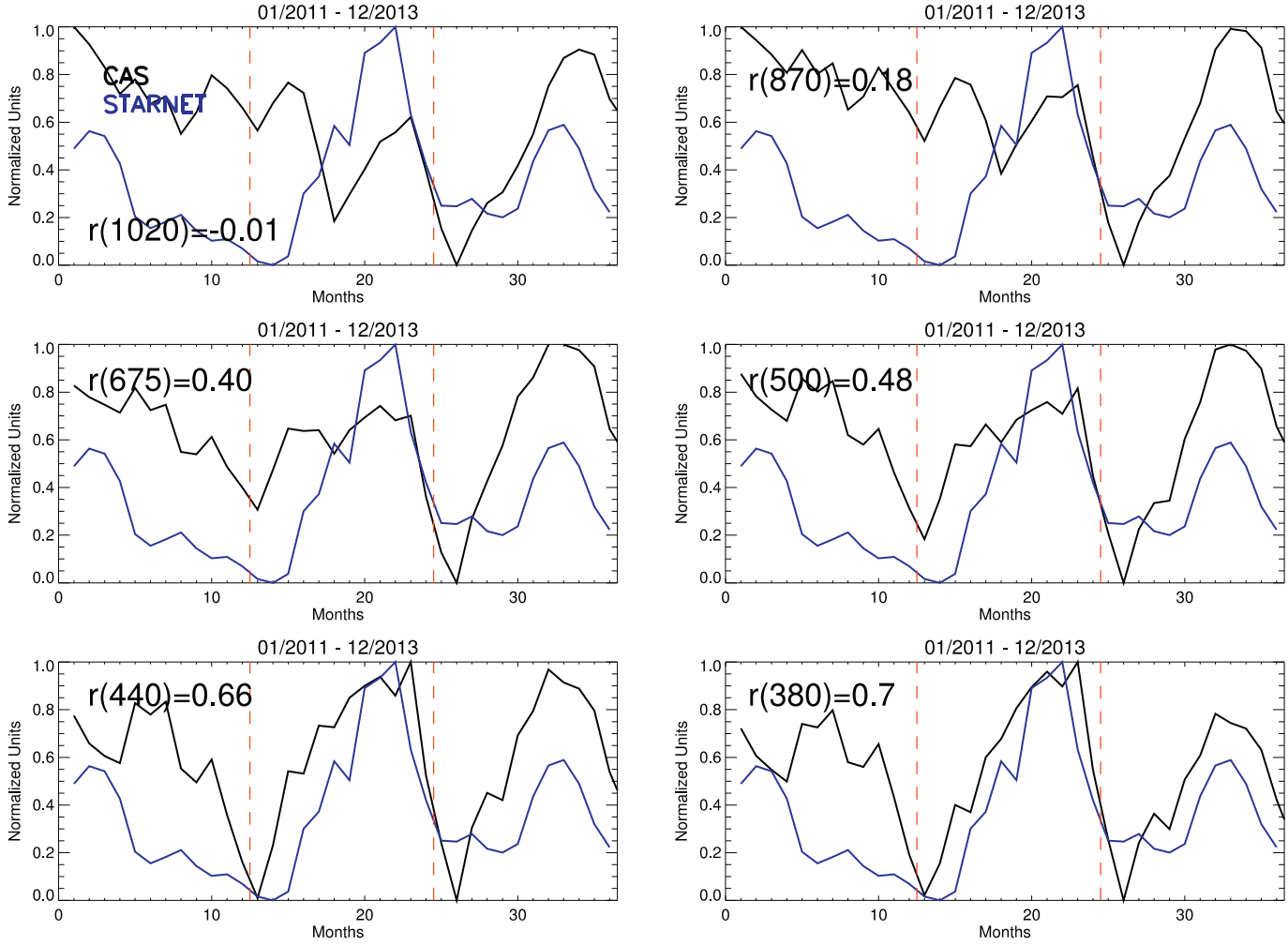

Fig. 17. Average monthly of number of lightning recorded for an area between 3000 and 18,000 km away from CASLEO (January 2011 to December 2013, blue color) with a moving average of 3 points. The black curve is the PG monthly average (3-point moving average) of Fig. 16. Both curves were normalized [0,1].

no aerosol data recorded for this entire period of time at CASLEO Observatory. With respect to global effects, Harrison and Usoskin (2010) have already shown PG variations following the cosmic ray cycle (inverse to the solar activity cycle). However, to evaluate this point, longer time series from CASLEO station are needed.

The spectral analysis of the PG variability shows that the important oscillations are the annual, diurnal and 165-day. From these, the AO and diurnal oscillation are frequently reported in the literature. Assuming that the 165-day oscillation can be interpreted as a quasi-semiannual oscillation (quasi-SAO) and considering that our present study shows the importance of convective processes on our PG measurements, then it is possible to suggest that the existence of this quasi-SAO may be related to local variation of aerosol. We performed the same wavelet analysis to aerosol and meteorological parameters measured at CAS. However, the 165-day oscillation does not appear in those time series. On the other hand, there is the possibility that the PG measurements also contain the influences of external physical sources that are not clearly observed in our analysis. Thus, further analysis, using data obtained at different geographical locations, is required to understand why the 165-day oscillation is observed in the PG measurements.

5. Summary

In this paper we have investigated the atmospheric electric variation, through potential gradient measurements, during fair weather conditions measured in the Andes Mountain of Argentina and the main physical divergences when compared with the Carnegie curve. The results showed the possibility of providing reliable standard curves of the atmospheric electric field in fair weather conditions. The annual standard curve closely resemble the 'universal' Carnegie curve (r = 0.94). However, some deviations were found, which are possible associated to convective processes. These processes are more intense in summertime than in wintertime. It was also found that the long-term variation of the atmospheric electric field shows a clear seasonal variation opposite to the global distribution of thunderstorm. This opposite behavior can be associated to the aerosol load at CASLEO station, which is higher in summertime, and, after removing that influence, a similar pattern is found between both electric parameters (electric field and thunderstorms). In addition, the spectral analyses showed a diurnal, annual and 165-day oscillation in the atmospheric electric field time series. The correct identification of local effects is important to evaluate global effects on the electric field related to the global electric circuit.

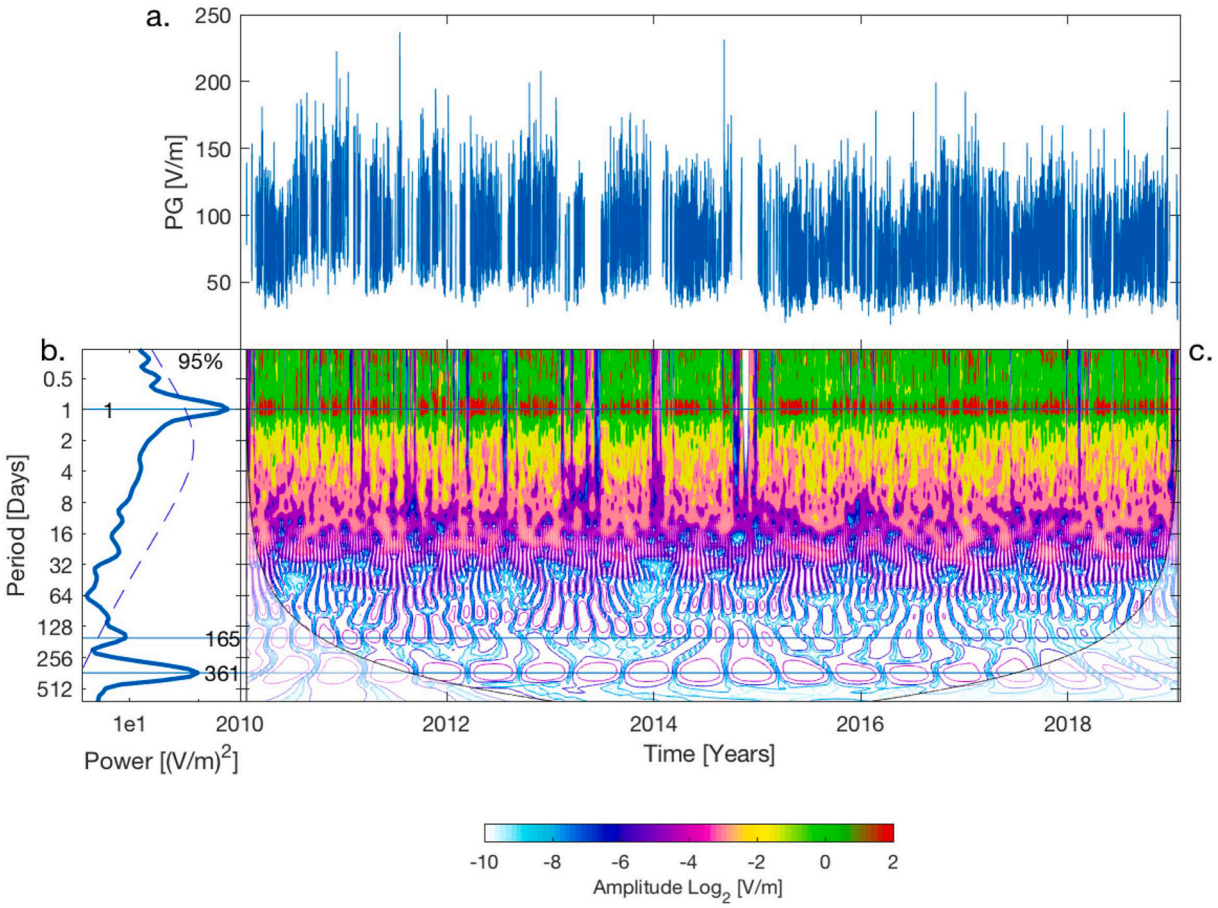

Fig. 18. (a) Hourly average of the PG amplitude. Gaps are missing data. (b) The global wavelet power spectrum. The horizontal lines indicate the most significant oscillations and the dashed curve is the 95% confidence level. (c) Contours in the time–period domain of the real part of the wavelet transform of the atmospheric electric field amplitude. The contours colors indicate the minimum and maximum magnitude, from white to red, of the matches between the phases of the time series and the wavelet. The white shadowed lateral edges are values within the cone of influence.

Declaration of Competing Interest

The authors declare that they have no known competing financial interests or personal relationships that could have appeared to influence the work reported in this paper.

Acknowledgements

Jose Tacza was supported by the PNPD/CAPES funding agency. Jose Tacza and Jean-Pierre Raulin thank funding agencies CNPq (projects: 422253/2016-2 and 312066/2016-3) and CAPES (project 88881.310386/2018-01). The authors thank AERONET principal investigators and their staff for establishing and maintaining the AERONET sites used in this investigation. This work is partially based on data acquired at Complejo Astronómico El Leoncito, operated under agreement between the Consejo Nacional de Investigaciones Científicas y Técnicas de la República de Argentina and the National Universities of La Plata, Córdoba and San Juan.

References

Adlerman, E.J., Williams, E.R., 1996. Seasonal variation of the global electrical circuit. J. Geophys. Res. 101 (D23), 29679–29688.
Anisimov, S.V., Galichenko, S.V., Shikhova, N.M., 2012. Formation of electrically active layers in the atmosphere with temperature inversion. Atmos. Oceanic Phys. 48 (4), 391–400.
Anisimov, S.V., Afinogenov, K.V., Shikhova, N.M., 2014. Dynamics of undisturbed mid-latitude atmospheric electricity: from observations to scaling. Radiophys. Quant. Elect. 56 (11–12).
Anisimov, S.V., Galichenko, S.V., Mareev, E.A., 2017. Electrodynamic properties and height of atmospheric convective boundary layer. Atmos. Res. 194, 119–129.
Anisimov, S.V., Galichenko, S.V., Aphinogenov, K.V., Prokhorchuk, A.A., 2018. Evaluation of the atmospheric boundary-layer electrical variability. Bound.-Layer Meteorol. 167 (2), 327–348.
Boyouk, N., Leon, J.-F., Delbarre, H., Podvin, T., Deroo, C., 2010. Impact of the mixing boundary layer on the relationship between PM2.5 and aerosol optical thickness. Atmos. Environ. 44, 271–277.
Burns, G.B., Tinsley, B.A., Frank-Kamenetsky, A.V., Troshichev, O.A., French, W.J.R., Klekociuk, A.R., 2012. Monthly diurnal global atmospheric circuit estimates derived from Vostok electric field measurements adjusted for local meteorological and solar wind influences. J. Atmos. Sci. 69 (6), 2061–2082.
Burns, G.B., Frank-Kamenetsky, A.V., Tinsley, B.A., French, W.J.R., Grigioni, P., Camporeale, G., Bering, E.A., 2017. Atmospheric global circuit variations from Vostok and Concordia electric field measurements. J. Atmos. Sci. 74 (3), 783–800.
Canton, J., 1753. Electrical experiments with an attempt to account for their several phenomena; together with some observations on thunder-clouds. Philos. Trans. R. Soc. Lond. 48 (1753–1754), 350–358.
Ceca, L.S.D., Ferreyra, M.F.G., Lyapustin, A., Chudnovsky, A., Otero, L., Carreras, H., Barnaba, F., 2018. Satellite-based view of the aerosol spatial and temporal variability in the Cordoba region (Argentina) using over ten years of high-resolution data. J. Photogram. Remote Sens. 145, 250–267.
Christian, H.J., Blakeslee, R.J., Boccipio, D.J., Boeck, W.L., Buechler, D.E., Driscoll, K.T., Goodman, S.J., Hall, J.M., Koshak, W.J., Mach, D.M., Stewart, M.F., 2003. Global frequency and distribution of lightning as observed from space by the Optical Transient Detector. J. Geophys. Res. 108 (D1), 4005.
Cobb, W.E., 1968. The atmospheric electric climate at Mauna Loa Observatory, Hawaii. J. Atmos. Sci. 25, 470–480.
Garcia, M.E., Ceca, L.S.D., Micheletti, M.I., Piacentini, R.D., Ordano, M., Reyes, N.J.F., Buedo, S., Gonzalez, J.A., 2018. Environ. Sci. 5 (3), 173–194.

Grinsted, A., Moore, J.C., Jevrejeva, S., 2004. Application of the cross wavelet transform and wavelet coherence to geophysical time series. Nonlinear Process. Geophys. 11, 561–566. https://doi.org/10.5194/npg-11-561-2004.
Gupta, P., Christopher, S.A., 2008. Seven year particulate matter air quality assessment from surface and satellite measurements. Atmos. Chem. Phys. 8, 3311–3324.
Gurmani, S.F., Ahmad, N., Tacza, J., Hussain, T., Shafaq, S., Iqbal, T., 2020. Comparative analysis of local and global atmospheric electric field at the Northern Pakistan. J. Atmos. Sol. Terr. Phys. 206, 105326.
Haldoupis, C., Rycroft, M., Williams, E., Price, C., 2017. Is the "Earth-ionosphere capacitor" a valid component in the atmospheric electric circuit? J. Atmos. Sol. Terr. Phys. 164, 127–131.
Harrison, R.G., 2003. Twentieth-century atmospheric electrical measurements at the observatories of Kew, Eskdalemuir and Lerwick. Weather 58, 11–19.
Harrison, R.G., 2006. Urban smoke concentrations at Kew, London, 1898 – 2004. Atmos. Environ. 40, 3327–3332.
Harrison, R.G., 2013. The Carnegie Curve. Surv. Geophys. 34 (2), 209–232.
Harrison, R.G., Aplin, K.L., 2002. Mid-nineteenth century smoke concentrations near London. Atmos. Environ. 36, 4037–4043.
Harrison, R.G., Nicoll, K.A., 2018. Fair weather criteria for atmospheric electricity measurements. J. Atmos. Sol. Terr. Phys. 179, 239–250.
Harrison, R.G., Usoskin, I., 2010. Solar modulation in surface atmospheric electricity. J. Atmos. Sol. Terr. Phys. 72 176–172.
Holben, B.N., Eck, T.F., Slutsker, I., 1998. AERONET – a federated instrument network and data archive for aerosol characterization. Remote Sens. Environ. 66 (1), 1–16.
Imyanitov, I.M., 1957. Pribory i metody dlya izucheniya elektrichestva atmosfery (Instruments and methods for studying the electricity of the atmosphere). Gostekhizdat, Moscow.
Israël, H., 1959. Atmospheric electrical agitation. Q. J. R. Meteorol. Soc. 85 (364), 91–104.
Israelsson, S., Tammet, H., 2001. Variation of fair weather atmospheric electricity at Marsta Observatory, Sweden, 1993-1998. J. Atmos. Sol. Terr. Phys. 63, 1693–1703.
Jeeva, K., Gurubaran, S., Williams, E.R., Kamra, A.K., Sinha, A.K., Guha, A., Selvaraj, C., Nair, K.U., Dhar, A., 2016. Anomalous diurnal variation of atmospheric potential gradient and air-Earth current density observed at Maitri, Antarctica. J. Geophys. Res.-Atmos. 121, 1–19.
Kamogawa, M., Suzuki, Y., Sakai, R., Fujiwara, H., Tori, T., Kakinami, Y., Watanabe, Y., Sato, R., Hashimoto, S., Okochi, H., Miura, K., Yasuda, H., Orihara, Y., Suzuki, T., 2015. Diurnal variation of atmospheric electric field at the summit of Mount Fuji, Japan, distinctly from the Carnegie curve in summertime. Geophys. Res. Lett. 42, 3019–3023.
Kasemir, H.W., 1972. Atmospheric electric measurements in the Arctic and the Antarctic. Pure Appl. Geophys. 100 (1), 70–80.
Kubicki, M., Odzimek, A., Neska, M., Berlinski, J., Michnowski, S., 2016. First measurements of the Earth's electric field at the Arctowski Antarctic Station, King George Island, by the new polish atmospheric electricity observation network. Acta Geophysica 64 (6), 2630–2649.
Liu, Y., San Liang, X., Weisberg, R.H., 2007. Rectification of the Bias in the Wavelet Power Spectrum. J. Atmos. Ocean. Technol. 24 (12), 2093–2102. https://doi.org/10.1175/2007JTECHO511.1.
Lopes, F.M., Silva, H.G., Bennett, A.J., Reis, A.H., 2017. Global electric circuit research at Graciosa Island (ENA-ARM facility): first year of measurements and ENSO influences. J. Electrost. 87, 203–2011.
Lucas, G.M., Thayer, J.P., Deierling, W., 2017. Statistical analysis of spatial and temporal variations in atmospheric electric fields from a regional array of field mills. J. Geophys. Res.-Atmos. 122, 1158–1174.
Macotela, E.L., Clilverd, M., Manninen, J., Moffat-Griffin, T., Newnham, D.A., Raita, T., Rodger, C.J., 2019. D-region high-latitude forcing factors. J. Geophys. Res. Space Physics 124, 765–781. https://doi.org/10.1029/2018JA026049.
Marcz, F., Harrison, R.G., 2003. Long-term changes in atmospheric electrical parameters observed at Nagycenk (Hungary) and the UK observatories at Eskdalemuir and Kew. Ann. Geophys. 21, 2193–2200.
Markson, R., 1975. Atmospherical electrical detection of organized convection. Science 188, 1171–1177.
Markson, R., 1986. Tropical convection, ionospheric potentials and global circuit variation. Nature 320, 588–594.
Markson, R., 2007. The global circuit intensity: its measurements and variation over the last 50 years. Bull. Am. Meteorol. Soc. 88 (2), 223–242.
Markson, R., Ruhnke, L.H., Williams, E., 1999. Global scale comparison of simultaneous ionospheric potential measurements. Atmos. Res. 51, 315–321.
Marshall, T.C., Rust, W.D., Stolzenburg, M., Roeder, W.P., Krehbiel, P.R., 1999. A study of enhanced fair-weather fields occurring soon after sunrise. J. Geophys. Res. 104 (D20), 24455–24469.
Martins, V.S., Lyapsutin, A., de Carvalho, L.A.S., Barbosa, C.C.F., Novo, E.M.L.M., 2017. Validation of high-resolution MAIAC aerossol product over South America. J. Geophys. Res.-Atmos. 122, 7537–7559.
Mezuman, K., Price, C., Galanti, E., 2014. On the spatial and temporal distribution of global thunderstorm cells. Environ. Res. Lett. 9, 124023.
Morales, C.A., Anagnostou, E.N., 2003. Extending the capabilities of high-frequency rainfall estimation from geostationary-based satellite infrared via a network of long-range lightning observations. J. Hydrometeorol. 4 (2), 141–159.
Nichols, E., 1916. Investigation of atmospheric electric variations at sunrise and sunset. Proceed. Royal Soc. A 92 (642), 401–408.
Nicoll, K.A., Harrison, R.G., Silva, H.G., Salgado, R., Melgão, M., Bortoli, D., 2018. Electrical sensing of the dynamical structure of the planetary boundary layer. Atmos. Res. 202, 81–95.
Nicoll, K.A., Harrison, R.G., Barta, V., Bor, J., Brugge, R., Chillingarian, A., Chum, J., Georgoulias, A.K., Guha, A., Kourtidis, K., Kubicki, M., Mareev, E., Matthews, J., Mkrtchyan, H., Odzimek, A., Raulin, J.-P., Robert, D., Silva, H.G., Tacza, J., Yair, Y., Yaniv, R., 2019. A global atmospheric electricity monitoring network for climate and geophysical research. J. Atmos. Sol. Terr. Phys. 184, 18–29.
Parsons, J., Mazeas, W., 1753. Observations upon Electricity of the Air, made at the Chateau de Maintenon, during the months of June, July, and October, 1753. Philos. Trans. R. Soc. Lond. 48 (1753–1754), 377–384.
Peterson, M., Deierling, W., Liu, Ch., Mach, D., Kalb, Ch., 2017. A TRMM/GPM retrieval of the total generator current for the global electric circuit. J. Geophys. Res.-Atmos. 122, 10025–10049.
Price, C., 1993. Global surface temperatures and the atmospheric electric circuit. Geophys. Res. Lett. 20, 1363–1366.
Reddell, B.D., Benbrook, J.R., Bering, E.A., Cleary, E.N., Few, A.A., 2004. Seasonal variations of atmospheric electricity measured at Amundsen-Scott south Pole station. J. Geophys. Res. 109, A09308.
Reiter, R., 1971. Further evidence for impact of solar flares on potential gradient and air-Earth current characteristics at high mountain stations. Pure Appl. Geophys. 86 (1), 142–158.
Rycroft, M.J., Israelsson, S., Price, C., 2000. The global atmospheric electric circuit, solar activity and climate change. J. Atmos. Solar-Terr. Phys. 62, 1563–1576.
Rycroft, M.J., Harrison, R.G., Nicoll, K.A., Mareev, E.A., 2008. An overview of Earth's global electric circuit and atmospheric conductivity. Space Sci. Rev. 137 (1–4), 83–105.
Rycroft, M.J., Nicoll, K.A., Aplin, K.L., Harrison, R.G., 2012. Recent advances in global electric circuit between the space environment and the troposphere. J. Atmos. Sol. Terr. Phys. 90-91, 198–211.
Secker, P.E., 1975. The design of simple instrumentation for measurement of charge on insulating surfaces. J. Electrost. 1 (1), 27–36.
Silva, H.G., Conceição, R., Melgão, M., Nicoll, K., Mendes, P.B., Tlemçani, M., Reis, A.H., Harrison, R.G., 2014. Atmospheric electric field measurements in urban environment and the pollutant aerosol weekly dependence. Environ. Res. Lett. 9, 114025.
Smirnov, A., Holben, B.N., Savoie, D., Prospero, J.M., Kaufman, Y.J., Tanre, D., Eck, T.F., Slutsker, I., 2000. Relationship between column aerosol optical thickness and in situ ground based dust concentrations over Barbados. Geophys. Res. Lett. 27 (11), 1643–1646.
Smirnov, S.E., Mikhailova, G.A., Kapustina, O.V., 2012. Problem of the nature of the sunrise effect in diurnal variations in the electric field in Kamchatka: 1. Time variations in the electric field. Geomagn. Aeron. 52 (4), 507–512.
Stull, R.B., 1988. An Introduction to Boundary Layer Meteorology. Kluwer Academic Publishers, The Netherlands.
Tacza, J., Raulin, J.-P., Macotela, E., Norabuena, E., Fernandez, G., Correia, E., Rycroft, M.J., Harrison, R.G., 2014. A new south American network to study the atmospheric electric field and its variations related to geophysical phenomena. J. Atmos. Sol. Terr. Phys. 120, 70–79.
Tacza, J., Raulin, J.-P., Macotela, E.L., Norabuena, E.O., Fernandez, G., 2016. Atmospheric electric field variations and lower ionosphere disturbance during the total solar eclipse of 2010 July 11. Adv. Space Res. 58, 2052–2056.
Tacza, J., Raulin, J.-R., Mendonca, R.R.S., Makhmutov, V.S., Marun, A., Fernandez, G., 2018. Solar effects on the atmospheric electric field during 2010-2015 at low latitudes. J. Geophys. Res.-Atmos. 123, 1–10.
Tacza, J., Raulin, J.-P., Macotela, E., Marun, A., Fernandez, G., Bertoni, F.C.P., Lima, L.M., Samanes, J., Buleje, Y., Correia, E., Alves, G., Makita, K., 2020. Local and global effects on the diurnal variation of the atmospheric electric field in South America by comparison with the Carnegie curve. Atmos. Res. 240, 104938.
Tammet, H., 2009. A joint dataset of fair-weather atmospheric electricity. Atmos. Res. 91, 194–200.
Torrence, C., Compo, G., 1998. A practical guide to wavelet analysis. Bull. Am. Meteorol. Soc. 79, 61–78.
Torreson, O.W., Parkinson, W.C., Gish, O.H., Wait, G.R., 1946. Ocean Atmospheric-Electric Results (Scientific Results of Cruise VII of the Carnegie during 1928–1929 under Command of Captain J.P. Ault, vol3). Researches of the Department of Terrestrial Magnetism. Carnegie Institution of Washington Publication, pp. 568.
Videla, F.C., Barnaba, F., Angelini, F., Cremades, Pablo, Gobbi, G.P., 2013. The relative role of Amazonian and non-Amazonian fires in building up the aerosol optical depth in South America: a five year study (2005-2009). Atmos. Res. 122, 298–309.
Wang, J., Christopher, S.A., 2003. Intercomparison between satellite-derived aerosol optical thickness and PM 2.5 mass: Implications for air qualities studies. Geophys. Res. Lett. 30 (21), 2095.
Whipple, F.J.W., 1929. On the association of the diurnal variation of electric potential gradient in fine weather with the distribution of thunderstorms over the globe. Q. J. R. Meteorol. Soc. 55, 1–17.
Williams, E.R., 1992. The Schumann Resonance: a Global Tropical Thermometer. Science

256, 1184–1187.
Williams, E.R., 2009. The global electric circuit: a review. Atmos. Res. 91, 140–152.
Williams, E., Mareev, E., 2014. Recent progress on the global electric circuit. Atmos. Res. 135-136, 208–227.
Wilson, C.T.R., 1903. Atmospheric electricity. Nature 68, 101–104.
Wilson, C.T.R., 1921. Investigations on lightning discharges and on the electric field of thunderstorms. Philos.Trans. Roy. Soc. London 73–115 221A.
Yaniv, R., Yair, Y., Price, C., Katz, S., 2016. Local and global impacts on the fair-weather electric field in Israel. Atmos. Res. 172-173, 119–125.
Yaniv, R., Yair, Y., Price, C., Mkrtchyan, H., Lynn, B., Reymers, A., 2017. Ground-based measurements of the vertical E-field in mountainous regions and the “Austausch” effect. Atmos. Res. 189, 127–133.